ResearchGate

See discussions, stats, and author profiles for this publication at: https://www.researchgate.net/publication/385210157

A novel carbon quantum dot (CQD) synthesis method with cost-effective reactants and a definitive indication: Hot bubble synthesis (HBBBS)

Article *in* Journal of Science Advanced Materials and Devices · October 2024

DOI: 10.1016/j.jsamd.2024.100797

CITATION
1

READS
65

4 authors:



Beste Dipçin
Acıbadem University
3 PUBLICATIONS **2** CITATIONS
SEE PROFILE



Bora Güvendiren
Acıbadem University
3 PUBLICATIONS **2** CITATIONS
SEE PROFILE



Selçuk Birdoğan
Sabancı University Nanotechnology Research and Application Center
12 PUBLICATIONS **169** CITATIONS
SEE PROFILE



Bukem Tanoren
Acıbadem University
34 PUBLICATIONS **152** CITATIONS
SEE PROFILE

All content following this page was uploaded by Beste Dipçin on 01 November 2024.

The user has requested enhancement of the downloaded file.

Journal of Science: Advanced Materials and Devices 9 (2024) 100797

Contents lists available at ScienceDirect

Journal of Science: Advanced Materials and Devices

journal homepage: www.elsevier.com/locate/jsamd

Research article

A novel carbon quantum dot (CQD) synthesis method with cost-effective reactants and a definitive indication: Hot bubble synthesis (HBBBS)

Beste Dipcin [a,b,*], Bora Guvendiren [b,c], Selcuk Birdogan [d], Bukem Tanoren [b,e]

[a] Acibadem University, Faculty of Engineering and Natural Sciences, Department of Molecular Biology and Genetics, Istanbul, 34752, Atasehir, Turkey
[b] ACU Biomaterials A and R Center, Acıbadem Mehmet Ali Aydınlar University (ACU), Istanbul, 34752, Atasehir, Turkey
[c] Acibadem University, Faculty of Engineering and Natural Sciences, Department of Biomedical Engineering, Istanbul, 34752, Atasehir, Turkey
[d] Sabanci University SUNUM Nanotechnology Research and Application Center, Istanbul, 34956, Turkey
[e] Acibadem University, Faculty of Engineering and Natural Sciences, Department of Natural Sciences, Istanbul, 34752, Atasehir, Turkey

ARTICLE INFO

Keywords:
Carbon nanostructures
Quantum dots
Carbon quantum dots
Bottom-up approaches
Reaction indication

ABSTRACT

Carbon quantum dots (CQDs) are carbon-based biocompatible quantum dots that have low toxicity, are more soluble in water, have broad application areas, and the surface modification of these can be performed easily. In this study, we present a new CQD synthesis method with cost-effective reactants that can be easily found in laboratories are used. Besides, there is a definitive indication (bubble) for CQD production, unlike the other methods in the literature. The purification method of the CQDs was also optimized in this study. In the beginning of the synthesis, 3 times centrifugation (x3 CF) of the mixture was performed and the optimization of the purification method indicated that x3 CF before 3 days of dialysis membrane tubing (x3 CF & 3 DM) resulted in the formation of the purest CQDs. The characterization of the CQDs was done utilizing UV–VIS spectrophotometer, Fourier Transfer Infrared Spectroscopy (FT-IR), Zetasizer, fluorescence microscopy, Dynamic Light Scattering (DLS), Scanning Electron Microscope (SEM), Energy Dispersive Spectroscopy (EDS), and Transmission Electron Microscopy (TEM). It was concluded that the CQD formation depended on the mixing of sulphuric acid:acetone (2:1) ratio in a hot (140–165 °C) and an inert environment, and bubble coverage of the mixture surface (30–60 s). The bubble formation due to the reaction between sulphuric acid and pure acetone at high temperatures gives the developed method's name of "Hot Bubble Synthesis" (HBBBS).

1. Introduction

Quantum dots (QDs) are semiconductor nanocrystals that have a diameter between 1–10 nm, and have unique optical properties resulting from the quantum confinement effect [1–4]. The quantum confinement effect is a condition that applies to QDs when their Bohr radius is less than the De Broglie wavelength of an electron, which is ≈ 10 nm [5]. When the radius of QDs is less than 10 nm, all of the electron–hole pairs (exciton) are confined within three dimensions such that the magnitude of their attraction forces are neglected which induces the phenomenon known as quantum confinement [6,7]. Moreover, this phenomenon affects QDs' optical and electrical behavior [7]. More precisely, this phenomenon affects the energy band gaps of the QDs which determines their absorption and emission spectra [8].

QDs have high quantum yield (QY), size-tunable light emission spectra, broad excitation spectra, strong fluorescent intensity, and good chemical and light stability (photostability) that delays their photobleaching time [1,2,9]. QDs are made of inorganic or organic materials and the organic material-based QDs such as carbon quantum dots (CQDs), and graphene quantum dots (GQDs) are more biocompatible compared to inorganic QDs [10].

Carbon quantum dots (CQDs) (also named carbon dots in some studies) are carbon-based nanostructures that are considered to be biocompatible organic QDs with low toxicity and higher solubility in water; also, the surface modification is easier to perform compared to that of inorganic QDs [11,12]. Thanks to these properties, they are utilized in biological applications as catalysts [13], as bioimaging agents [14,15], as antimicrobial agents [16], in optoelectronic devices [17], in chemical sensors [18], in LEDs [19], in drug delivery systems [20], and in biosensing [21–23] or as supercapacitors [24]. The QD synthesis methods (appropriate for CQDs) are clas-

* Corresponding author at: Acibadem University, Faculty of Engineering and Natural Sciences, Department of Molecular Biology and Genetics, Istanbul, 34752, Atasehir, Turkey.
E-mail addresses: beste.dipcin@live.acibadem.edu.tr (B. Dipcin), bora.guvendiren@live.acibadem.edu.tr (B. Guvendiren), selcuk.birdogan@sabanciuniv.edu (S. Birdogan), bukem.tanoren@acibadem.edu.tr (B. Tanoren).
Peer review under responsibility of Vietnam National University, Hanoi.

https://doi.org/10.1016/j.jsamd.2024.100797
Received 7 August 2024; Received in revised form 23 September 2024; Accepted 27 September 2024
Available online 24 October 2024
2468-2179/© 2024 Vietnam National University, Hanoi. Published by Elsevier B.V. This is an open access article under the CC BY-NC-ND license (http://creativecommons.org/licenses/by-nc-nd/4.0/).

sified into two main approaches which are top-down and bottom-up approaches [25,26]. Top-down approaches tend to break down the bulk materials which form small molecules that polymerize into CQDs [26]. On the other hand, in bottom-up approaches, CQD precursors, which are small molecules, tend to polymerize and self-assemble to form intermediate macromolecules that are subjected to decomposition and carbonization to form CQDs [26]. For the synthesis of pure or modified (processed) CQDs; the submerged arc discharge in water [27], laser ablation [28], electrochemical [29], thermal [30], hydrothermal [31], microwave-assisted [32], microwave-assisted hydrothermal [33], and hot injection [34] synthesis methods were used.

In these synthesis methods, the formation of CQDs is mostly understood from the color change (a relative feature), and the synthesis is terminated, or its duration is determined accordingly [35]. Additionally, the materials used in stated QD synthesis methods such as graphite electrodes, are generally materials that cannot be found in every laboratory [27,28], or the synthesis is carried out in an autoclave at very high temperatures [31], and for a very long time [36]. Therefore, such necessities in the conventional synthesis methods reduce the applicability of CQD synthesis in every laboratory.

The most commonly used methods for the purification of CQDs are centrifugal washing using deionized water, filtration through the dialysis membrane, or filtration through the dialysis membrane after centrifugation [37]. Dialysis membranes with a molecular weight of 500–3500 Da (0.5–3.5 kDa) are generally used for purifying CQDs by filtering them through the dialysis membrane [34,35,37]. Even though filtration through the dialysis membrane approach seems to work, the purification methods' optimization for CQDs is not generally presented in the literature.

Here, we present a bottom-up approach-based method that has an explicit and easy-to-observe indication (bubble formation) that does not only depend on color change, is rapid and controllable, has an optimized purification method for CQD synthesis which can be done with reactants present in almost every laboratory (Fig. 1).

2. Materials, instruments & methods

2.1. Materials & instruments

2.1.1. Materials

Sulphuric acid (95%–98%) was obtained from Sigma-Aldrich (St. Louis, Missouri, USA), acetone (≥99.5% purity) was obtained from ISOLAB (Istanbul, Arnavutkoy, Turkey) and sodium hydroxide pellets (98% purity) were obtained from ThermoFisher Scientific (Waltham, Massachusetts, USA) were used. Throughout the experiments, all dilutions were done with ultra-pure deionized water (18MU Direct-Q water purification system, Millipore Inc., Bedford, MA, USA). For the purification of CQDs, the dialysis tubing membrane (MWCO: 1 kDa) was obtained from Repligen (Massachusetts, USA).

2.1.2. Instruments

The following instruments were utilized in the characterization studies: UV–VIS spectrophotometer (Shimadzu, UV-2600, Japan), fluorescent microscopy (Zeiss, Axio Observer.Z1/7, Germany), Cary Eclipse Fluorescence Spectrophotometer (Agilent, USA), Fourier Transform Infrared Spectroscopy (FT-IR) (Nicolet iS10, Thermo Fisher, USA), Zetasizer Nano (Malvern, England), Dynamic Light Scattering (DLS) (DynaPro Nanostar, Wyatt Technology, USA), Scanning Electron Microscopy (SEM) (Thermo Scientific™ Quattro ESEM, USA), Atomic Resolution Analytical Electron Microscope for Transmission Electron Microscopy (TEM) imaging (Jeol ARM200F, China).

2.2. Methods

2.2.1. Carbon quantum dots (CQDs) synthesis

The synthesis of CQDs was carried out within the fume hood. Initially, 5 mL of sulphuric acid (95%–98%) and 2.5 mL of acetone (≥98%) (sulphuric acid to acetone ratio: 2/1) were mixed within a one-neck 100 mL flask which was attached to a 250 mm reflux condenser. Before the chemicals were refluxed, the reaction flask was kept at a stable temperature by the silicon bath. In addition, the reaction environment was kept inert with N_2 gas, and the temperature was checked with the probe inserted into the silicone bath. The setup is given in Fig. 1. The silicone temperature was set to 165 °C and stirred between 300–500 rpm to establish a homogeneous temperature distribution around the reaction flask.

Through the temperature rise from room temperature to 165 °C, the reaction color changed from clear to yellow at 80–100 °C, and from yellow to black at 150–160 °C. The color change into black can be considered as the indication of the dehydration reaction between acetone and sulphuric acid, represented in Fig. 2. This reaction is supported by the study of Kane, Timonen & Leu, in which they concluded that the reaction between sulfuric acid and acetone [38] leads to the formation of carbon-based nanostructures such as graphenes, carbon nanotubes or CQDs [39–41].

As the reaction reached around 165 °C, bubble formation on the surface of the mixture can be observed. At this critical moment, the reaction flask was slowly removed from the silicon bath after 30–60 s when the mixture surface was surrounded with bubbles, cooled down to room temperature naturally, and was neutralized with NaOH. The reaction solution was centrifuged at 6000 rpm for 10–15 min. After being centrifuged, the supernatant was removed and water-soluble CQD aggregates were obtained. The vessels containing CQD aggregates were lyophilized to remove any water content within the tubes.

Characterization of CQDs

The characterization of materials that were taken out of the hot environment right after the first bubble formation and 30–60 s after the mixture surface was surrounded by bubbles were performed; and the characterization results of the materials are presented in Fig. 4 and from Fig. 5 to Fig. 18 respectively. For the characterization of the materials that were taken out of the hot environment 30–60 s after the mixture surface was surrounded by bubbles, different concentrations, and purification methods were used.

2.2.2. UV–VIS spectrophotometry & photoluminescence (PL) analysis

CQD solutions were prepared with different concentrations (3 mg/mL, 1 mg/mL, 500 μg/mL, 200 μg/mL, 100 μg/mL, and 50 μg/mL) by dissolving the lyophilized CQD powder in ultra-pure deionized water (MiliQ). The absorbance peaks of the CQDs with different concentrations were determined by the spectrum (between 200–800 nm) analysis, obtained by UV–VIS Spectrophotometer instrument, taking MiliQ as the blank, and 0.001 as the threshold. The photoluminescence (PL) peak of the CQD sample with a concentration of 0.5 mg/mL and purification by centrifugation of 3 times, was obtained by Cary Eclipse Fluorescence Spectrophotometer.

2.2.3. Fluorescence microscopy

Fluorescence microscopy imaging was performed with the fluorescent microscope. The CQD samples dissolved in MiliQ, with different concentrations, were prepared on a clean microscope slide, and the samples were dried within the fume hood overnight before imaging. 365 nm wavelength was used for the imaging of CQDs, and the obtained images were analyzed with Zen Pro 3.6 software.

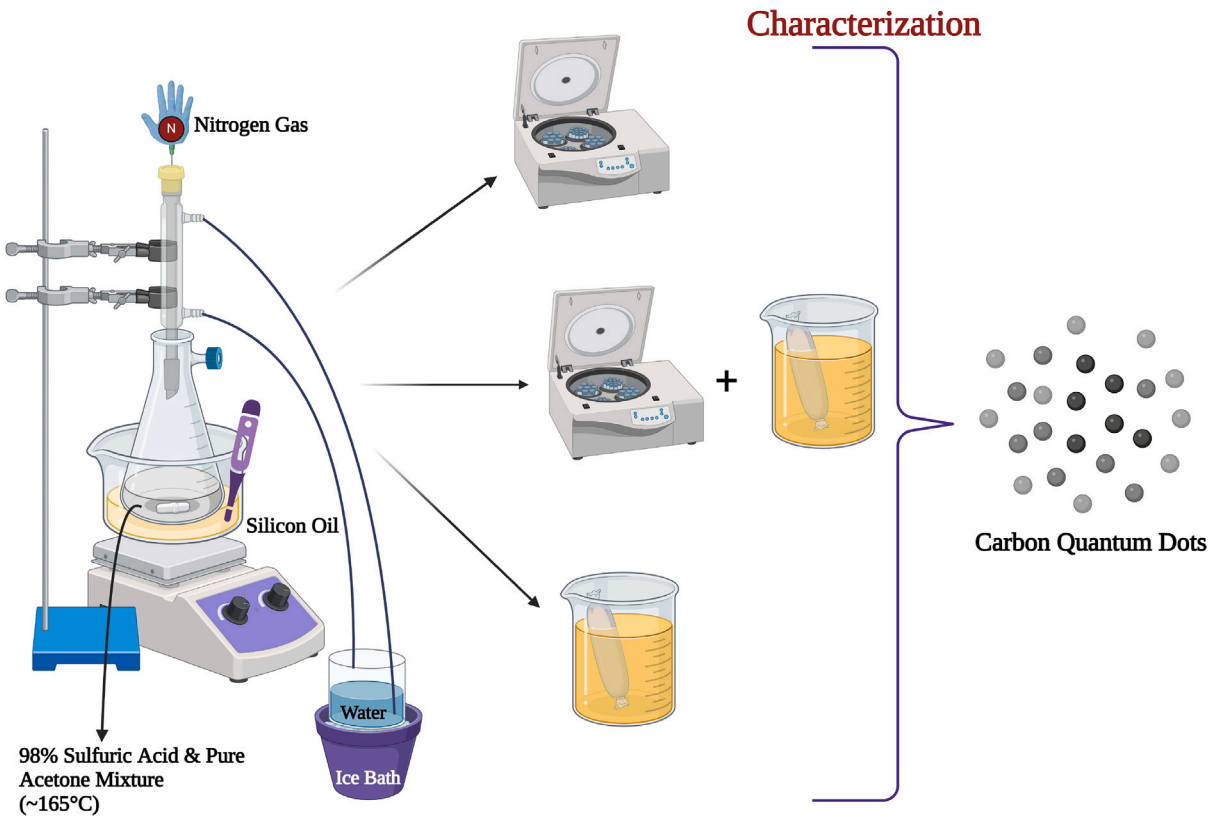


Fig. 1. Hot bubble synthesis (HBBBS) method schematic diagram. (Created with Biorender.com). Acetone was mixed with sulfuric acid in an inert environment maintained by a steady supply of nitrogen and homogeneous heating through a silicon bath. The reaction environment was heated to 165 °C with vapor being refluxed back. Once the reaction was returned to room temperature, it was neutralized with NaOH and purified via centrifugation or dialysis. The properties of the synthesized carbon quantum dots were then characterized.

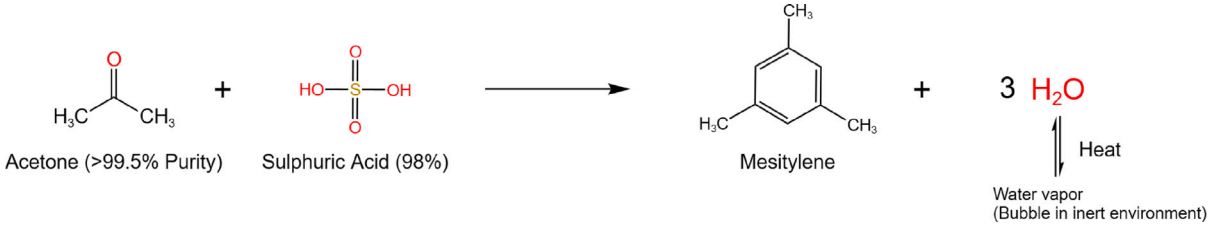


Fig. 2. Dehydration reaction between acetone and sulphuric acid around 165 °C to obtain the mesitylene molecule.

2.2.4. Fluorescence image analysis

The fluorescence images were obtained in ".czi" format with Zeiss Zen 3.7 software for 10X, 20X, and 40X objective lenses. During the acquisition of images, the same area of the sample was scanned. In the ".czi" image format, every pixel within the image is a representation of how many fluorescent signals were counted for that individual pixel. The workflow of the image analysis is presented in Fig. 3. The fluorescent image analysis was carried out for the membrane optimization and the comparison of purification methods.

Before the image analysis, the ".czi" images were pre-processed using Python's "pylibCZIrw" library, which allowed the extraction of pixel data from the ".czi" images. After gathering the pixel data from each image, the images were filtered to only segment the parts where the signal was obtained. The filtration was achieved by using the Laplace transformation. Using the Laplace transformation, masks were created for each image that replaced every part where there was not any signal with NaN. Afterward, using Python's "numpy" library's "nanmean" function, average signal intensity (or fluorescent signal count) was calculated for every image.

2.2.5. Fourier transform infrared spectroscopy (FT-IR)

For determining the chemical bonds of the CQDs, FT-IR was performed and the graphs of the transmittance percentage depending on the wavenumber were drawn using the GraphPad (Prism8) program.

2.2.6. Zeta potential analysis & dynamic light scattering (DLS) analysis

The surface charge of the CQDs was determined with Malvern Zetasizer Nano by mixing CQDs with a concentration of either 3 mg/mL or 0.2 mg/mL and 0.001M sodium chloride (NaCl) solution with a 1:9 ratio. The analysis was performed 3 times for each sample. The hydrodynamic radius of the CQDs was determined using a DLS, and the analysis was performed at least 3 times for each sample with a concentration of 3 mg/mL–0.05 mg/mL.

2.2.7. Scanning Electron Microscopy (SEM), Energy Dispersive Spectroscopy (EDS) & Transmission Electron Microscopy (TEM)

The morphological information and the elemental composition of the CQDs were obtained by SEM and EDAX Energy Dispersive Spectroscopy (EDS), respectively. Visualization of the CQDs was done under a high vacuum, using the Everhort-Thorley Detector (ETD). EDS was

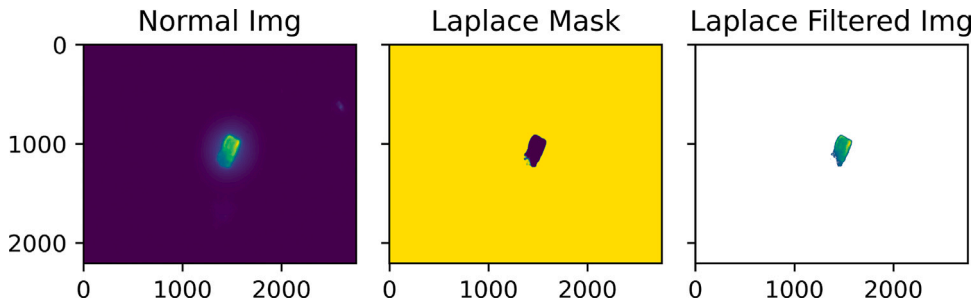


Fig. 3. Workflow of the image analysis. The normal image displayed here is the pixel data obtained from the ".czi" images. The Laplace mask image is obtained after the Laplace transformation of the normal image and thresholding were performed. The Laplace-filtered image is obtained by applying the Laplace mask on the normal image to obtain only the fluorescent signal-emitting parts.

performed for the CQDs with spherical morphology, localized by SEM. The EDAX EDS device was calibrated with aluminum (Al) and copper (Cu) standard samples of the APEX software automatically, and the EDS analysis was performed to get the spectrum of carbon (C), oxygen (O), sodium (Na), and sulfur (S). The elemental percentage was taken for both atomic and weight percentages.

The solid and purified CQDs were obtained by freeze-drying with the lyophilizer. Around 3–5 mg of CQDs were mixed with 2 mL of ethanol within 2 mL microcentrifuge tubes. Afterward, the aggregations were dissolved by 10 min of ultrasonication, and 5 μL of the CQD-ethanol solution was dropped onto the Lacey copper grid to obtain the TEM image using the Jeol ARM200F TEM device.

After the images of CQDs were obtained, the images were analyzed in the frequency domain by transforming with the Fourier transformation. The Fourier-transformed images were filtered using a high-pass filter and then, their inverse Fourier transform was taken. With the utilization of this method, the pixels belonging to CQDs remained within the filtered images. From these filtered images, the distances between individual carbon atoms were calculated.

2.2.8. Statistical analysis

Statistical analyses of Zeta potential analysis results (surface charge) were done for 2 different concentrations (3 mg/mL and 0.2 mg/mL) of the CQDs and for 3 different purification methods (x3 centrifugation, 3 days dialysis membrane tubing, and x3 centrifugation & 3 days dialysis membrane tubing). The graphics of the analyzed data were generated by the GraphPad (Prism8) program. Unpaired-one-tailed student's t-test (t-test with unequal variance) was used for the determination of statistically significant differences in the surface charges of CQDs. The level of statistical significance was set to $p < 0.05$. Two-way ANOVA Tukey's test was used for the elemental atomic% values, obtained by EDS, for different purification approaches, and the level of statistical significance was set to $p < 0.05$. The graphs were again generated by the GraphPad (Prism8) program.

2.2.9. Optimization of purification method for CQDs

For the purification method optimization, 3 different approaches were used; centrifugation of the CQDs 3 times (6000 rpm, 15 min each), dialysis membrane tubing (MWCO: 1 kDa) of the CQDs for 3 days, and a combination of these two purification methods. In the purification approach with dialysis membrane tubing for 3 days, the purification was done using MiliQ, and the water was changed every 6 h.

3. Results & discussion

3.1. CQD synthesis & characterization

In synthesizing the CQDs, the sulphuric acid:acetone ratio of 2:1 was found to be the most optimum ratio stated in a previous study [34]. Synthesis finished at approximately 150 °C when the mixture turned black, and no bubble formation was present, CQD characteristics were not able to be observed after 3 times centrifugation, and the characterization of the material was done utilizing FT-IR, SEM, and EDS (Fig. A.19). CQD aggregates purified by centrifugating them 3 times showed fluorescent properties (Fig. 4A) and the atomic percentage of the sodium and sulfur, considered as impurities, was found to be 15.75% (10.3% sodium, 5.45% sulfur), according to EDS analysis results (Fig. 4B) (Table 1). The undesired level of purified elements' (carbon and oxygen) percentage might have resulted from the transport of sodium and sulfur ions through electrostatic interactions in the sample that collapsed during centrifugation. It was determined that CQDs showed spherical morphology and formed large complexes, obtained by SEM (Fig. 4C). This complex formation can be explained by two phenomenons; the accumulation and agglomeration, which are two surfaces getting closer and entering into short-range thermodynamic interaction [42], and nano-sized particles coming together to reduce surface active energy, and by that increasing their size and reducing their surface area accordingly [43,44].

The diameter of the CQDs was obtained by TEM imaging after removing the mixture from the hot environment, immediately after the first bubble formation (when the bubbles do not cover the entire surface), and being purified by centrifugation 3 times and was found to be approximately 44.11 nm, which was larger than the value in literature (1−10 nm diameter) (Fig. 4D) [45,46]. Since the CQDs' size was larger than expected (Fig. 4D), they were suspected to be carbon aggregates or impurities. This large size of the material (Fig. 4D), and bubble alongside mesitylene molecule (precursor of CQD) formation occurs as a result of the dehydration reaction between sulfuric acid and acetone in a hot environment (Fig. 2) [38,47], it was decided to keep the mixture in a hot environment for 30–60 s after the mixture surface is fully covered with bubbles. Due to this dehydration reaction (Fig. 2), it can be assumed that the observation of more bubbles means the presence of more mesitylene molecules, therefore, the formation of more CQDs [38–41]. In the synthesis approach where the mixture was removed from the hot environment immediately after the first bubble was formed, an atom with a diameter of 340.6 picometers (pm) was detected, as can be seen in TEM image (Fig. 4D). We assume that this is the carbon atom, approved by the Van der Waals radius of carbon which is determined as 170 pm in literature [48]. The observation of a layer spacing of 340.6 pm in the TEM image (Fig. 4D) can be interpreted as the presence of a material of structure similar to graphene, since the similarity of CQDs and graphene was suggested before with FT-IR analysis, and CQDs consist of graphene in each layer and these layers have a characteristic gap of 0.340 nm (or 3.4 Å) due to the interaction of π-π orbitals between the aromatic rings [49,50].

The optimum incubation time at high temperatures was determined to be between 30–60 s after the bubbles surrounded all of the mixture surfaces. With a 30–60 s incubation time at high temperatures (145–165 °C), the pellet was obtained after centrifugation which enabled the purification of the mixture to obtain CQDs. Due to this optimization, experiments were performed with this incubation time.

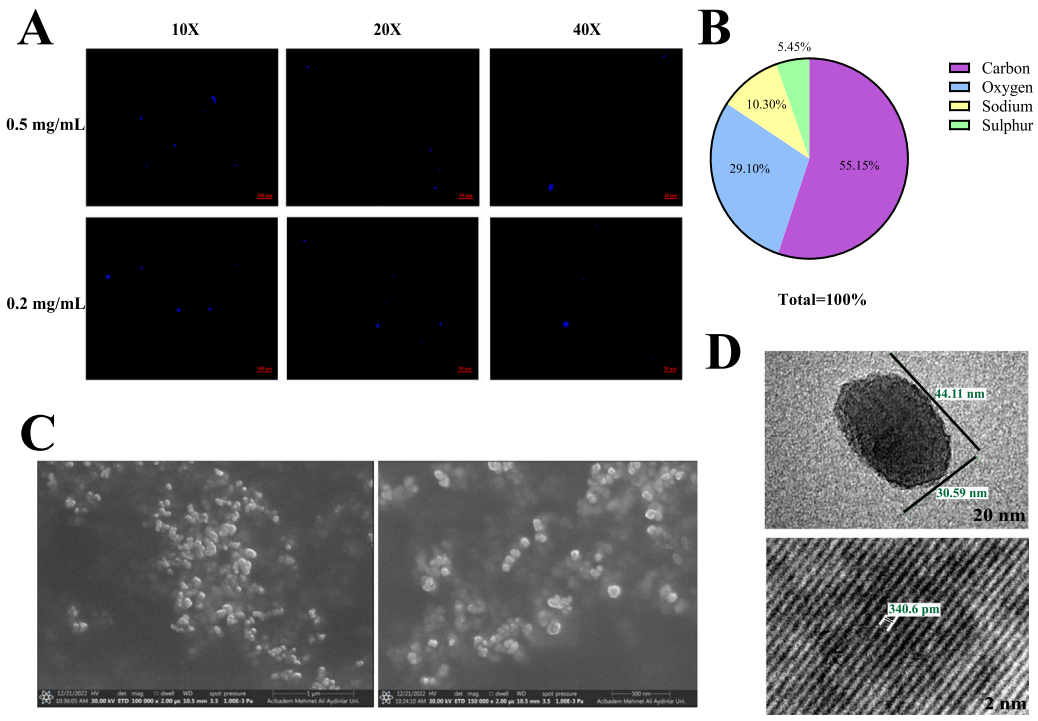


Fig. 4. Characterization of CQDs obtained right after the first bubble formation and purified by 3 times centrifugation. A: Fluorescence microscopy images of CQDs when excited with 365 nm. 10X scale bar: 100 μm, 20X scale bar: 50 μm, 40X scale bar: 20 μm. B: Elemental composition analysis of the CQD aggregates with EDS analysis. C: SEM images of CQD aggregates, scale bar: 1 μm and 500 nm. D: TEM images of CQD aggregates, scale bar: 20 nm and 2 nm.

Table 1
Elemental composition results with their standard deviation values obtained by EDS analysis of CQDs that were purified by centrifugation 3 times.

Analysis number	Atomic % Carbon	Atomic % Oxygen	Atomic % Sodium	Atomic % Sulfur
1	50.6 ± 0.092	29.8 ± 0.095	13.5 ± 0.074	6.1 ± 0.024
2	65.87 ± 0.075	25.13 ± 0.097	7.03 ± 0.073	1.97 ± 0.020
3	39.97 ± 0.095	32.37 ± 0.091	10.37 ± 0.072	8.00 ± 0.027

In the synthesis approach where the mixture was removed from the hot environment immediately after the first bubble was formed and subjected to the x3 CF purification method, the absorbance analysis was carried out with the UV–VIS spectrophotometer to confirm that CQDs were formed. The absorbance spectra of samples with 3, 1, and 0.5 mg/mL concentrations were not measurable in the absorbance analysis, however, the spectra of samples with 0.2, 0.1, and 0.05 mg/mL concentrations were measurable. The absorbance analysis of x3 CF showed that the peaks of these samples of 0.2, 0.1, and 0.05 mg/mL concentrations were recorded as 288, 286, and 285 nm respectively. Considering these results, a baseline for the purity of CQDs was chosen to be 293 nm [34]. The absorbance results, shown in (Fig. 5A) displayed an increase in the absorbance intensity at ≈ 290 nm, which meant that the absorbance results showed a correlation with literature and a similar synthesis approach was chosen [34,51,52]. It is theorized that the absorbance peaks around 290 nm were caused by π-π^* orbital transition owing to the sp^2 hybridization pattern of the C=C bond in the CQD structure [51]. On the other hand, the photoluminescence (PL) of the 0.5 mg/mL CQD sample was determined. The PL result (Fig. 5B) showed a red-shift in the fluorescent emission, in accordance with literature [34]. Furthermore, based on the PL result, it can also be deduced that the sample had a low polydispersity index since if the size distribution were heterogeneous, there would be both red-shift and blue-shift in fluorescent emissions [53].

The signals in the fluorescent microscopy images were thought to come from CQD aggregates, since the hydrodynamic diameters of the 0.5 mg/mL and 0.2 mg/mL samples were approximately 44 nm and 52 nm, respectively (Fig. 6). Besides, the diameter of the CQDs was found to be 44.11 nm by TEM (Fig. 4D) [54]. There was no correlation between the hydrodynamic radius and CQD concentration (Fig. 6). It was observed, as the concentration decreased, the hydrodynamic radius increased differing from the literature [55,56]. The polar interaction between the CQD and water might be the cause of CQDs being more prone to aggregation resulting in an increment in the hydrodynamic radius of CQDs, since their polar interactions with water, also, the time they are in the water, increase [56,57]. On the other hand, it is thought that organic solvents such as toluene could be used instead of inorganic solvents such as water for smaller hydrodynamic radius, since it is known that when QDs are dissolved in organic solvents they tend to have smaller hydrodynamic radius [56].

The surface charge values of the CQDs obtained by removing the mixture from the hot environment immediately after the first bubble formation and purified by centrifugation 3 times are presented in Table 2. CQDs that were purified by 3 times centrifugation with a concentration of 3 mg/mL and 0.2 mg/mL had the average surface charge of –42.60 ±0.88 and –19.57 ±1.11 mV, respectively (Fig. 7). The charge difference between these two concentrations was found to be statistically significant indicating as the concentration of the CQDs increased, the surface charge decreased. Since surface charge fairly depends on the particle size and generally increases with the particle size and concentration, the sample with a concentration of 3 mg/mL was bigger in size than the sample with a concentration of 0.2 mg/mL

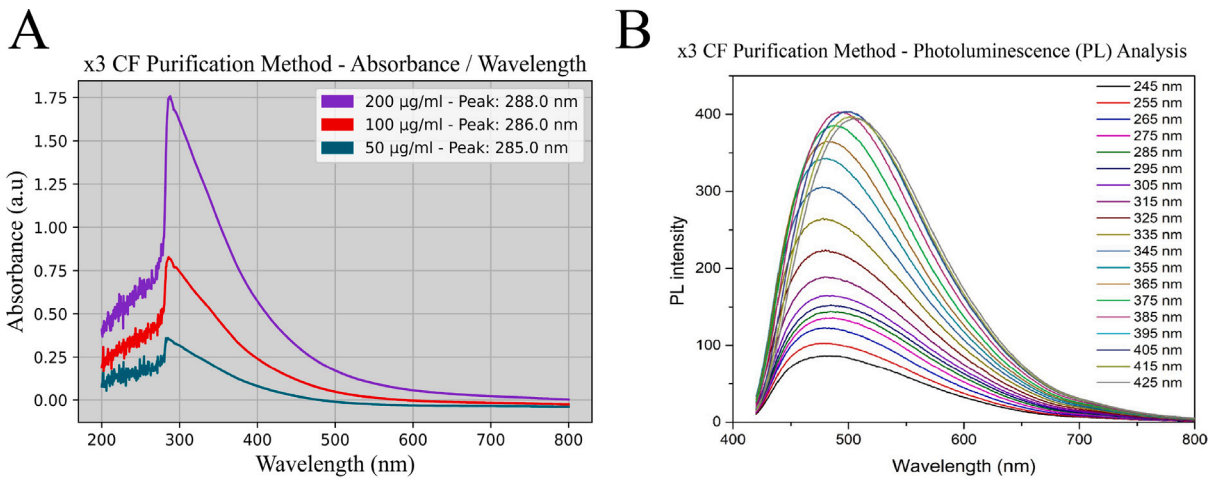


Fig. 5. The absorbance and PL analysis of CQDs purified with x3 CF purification method. A: Absorbance of CQDs, B: PL Analysis.

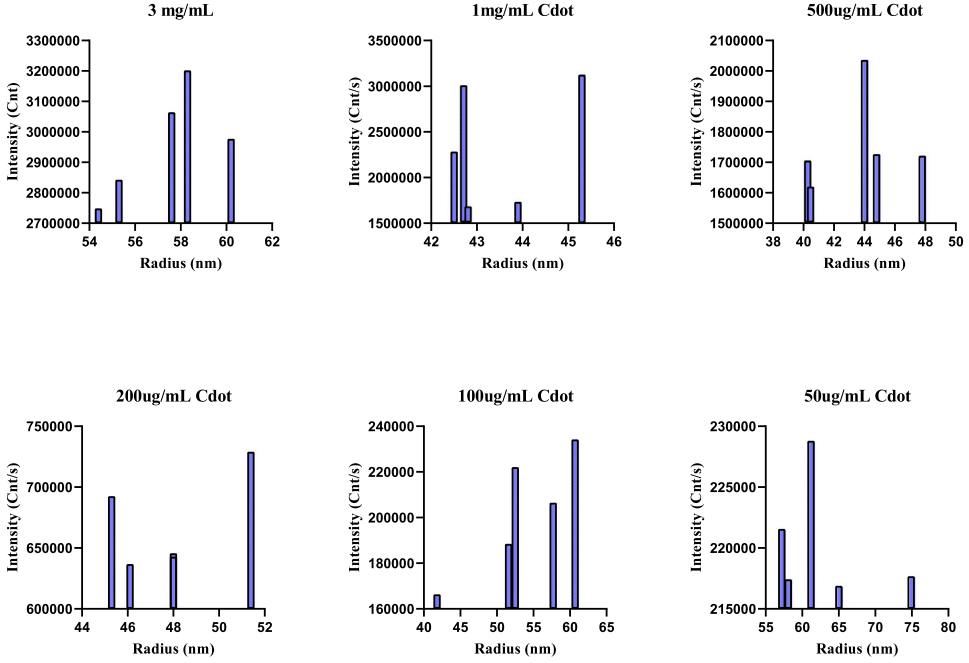


Fig. 6. Concentration-based hydrodynamic radii of the CQDs that were purified with the x3 CF method, obtained by DLS analysis.

(Fig. 6A), and the difference in the surface charge can be explained by that [58,59]. The negative surface charge of the CQDs can be a result of the carboxyl group presence on the surface of the CQDs which is supported by the FT-IR results (Fig. 6B) [60,61].

The 3380 cm^{-1} peak obtained from the FT-IR analysis corresponded to O-H in the alcohol class bond, 2954 cm^{-1} peak to alkane C-H bond, 1587 cm^{-1} peak to cyclic alkene (C=C) bond, 1434 cm^{-1} peak to the C-O-C (COO-) carboxylic acid bond, 1114 cm^{-1} peak to the C-O aliphatic ether bond, and 1040 cm^{-1} peak to either C-H or C-O bond (Fig. 7) [62–65]. Wavenumbers at 3380, 2954, 1434, 1114, 1040 cm^{-1} indicate the O-H, C-H, C-O-C, C-O, C-H/C-O bonds respectively and FT-IR analysis showed that these bonds are present on the surface of the CQDs [65]. Making these bond groups functional is really important in some application areas of the CQDs such as sensors, biosensors, and drug delivery systems [66]. The peak at the wavenumber of 1587 cm^{-1} which corresponded to the C=C bond (carbon–carbon cyclic alkene bond) suggests that the CQDs have a similar surface structure to graphene, and this result can be expected since the CQDs form due to the noncovalent π bond interactions between the graphene aromatic rings which are formed by the mesitylene molecules coming together [65].

3.2. Optimizing purification method for CQDs

For the optimization of the 3 DM purification method, samples taken from the dialysis membrane tubing at 0 h, 24 h, 48 h, and 72 h were imaged (Fig. 8). The images' fluorescent intensities were analyzed to select the best hour of purification (Fig. 9). The fluorescent image

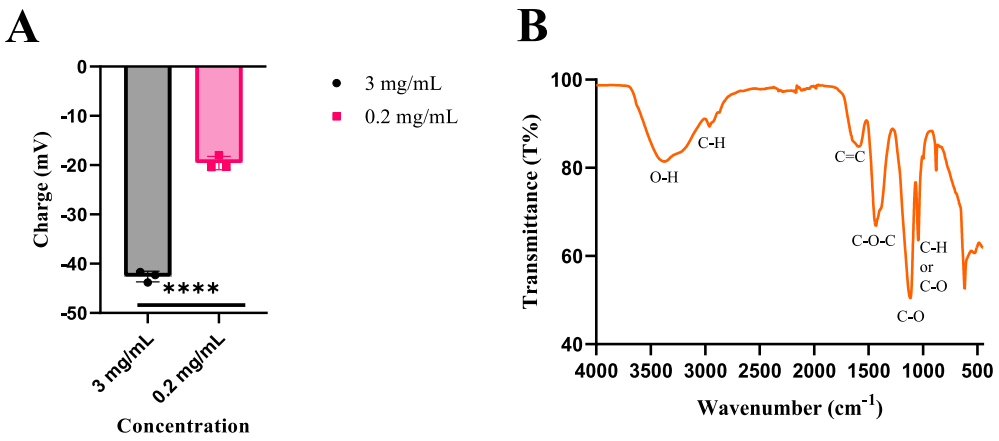


Fig. 7. Zeta Potential & FT-IR analysis data of CQD purified w/ 3 times centrifugation A: Zeta potential analysis, B: FT-IR analysis. (ns:non-significant, *p < 0.05, **p < 0.01, ***p < 0.001, ****p < 0.0001).

Table 2
Surface charge values of CQDs with different concentrations, purified by centrifugation 3 times.

Concentration of CQD	Purification method	Surface charge (mV)
3 mg/mL	Centrifugation (3 times)	−42.3
3 mg/mL	Centrifugation (3 times)	−43.8
3 mg/mL	Centrifugation (3 times)	−41.7
0.2 mg/mL	Centrifugation (3 times)	−20.3
0.2 mg/mL	Centrifugation (3 times)	−18.0
0.2 mg/mL	Centrifugation (3 times)	−20.4

analysis showed that the signal intensity was increased for all objective lenses after 24 h. However, after 48 h the fluorescent intensities were observed to be much lower when compared to the intensities at 24 h. The fluorescent intensities increased again at 72 h, although not as much as at the 24 h. Even though the fluorescent signal of the 24 h sample was high, it was also seen that the salt concentration was higher than the 72 h samples. From these findings, it was concluded that the 72 h purification time yielded the best result in terms of CQD purity for the 3 DM purification method.

For the comparison of purification methods, absorbance analysis of 200 μg/mL (0.2 mg/mL) samples was done, since, the best results were obtained for that concentration. The purity levels of CQDs were determined based on their absorbance differences by taking 293 nm wavelength as a baseline, which was done in a previous study to determine the purity of CQDs. The lowest peak absorbance difference to the baseline was observed in the x3 CF & 3 DM method (Fig. 10). Although the absorbance intensity of the sample with 3 DM purification method was high, the difference in peak absorbance to the baseline was significant when compared to other purification methods. The wavelengths in which the maximum absorbance values were obtained, and the magnitude of the absorbance intensities gave an idea about the purity and amount of CQDs present within the samples. Based on this claim, it can be suggested that the x3 CF & 3 DM purification method is the best method to purify the CQDs compared to other purification methods without leading to a significant decrease in signal.

To compare the purification methods further, samples with a concentration of 200 and 500 μg/mL (0.2 and 0.5 mg/mL) were prepared for fluorescent imaging (Figs. 11 and 12 respectively). The fluorescent intensities of the samples were assessed to determine the performance of the purification methods. The x3 CF & 3 DM purification method's sample with a concentration of 0.5 mg/mL and with 10X magnification had 3700, with 20X magnification had 3100, and with 40X magnification had 1400 counts; the sample with a concentration of 0.2 mg/mL and with 10X magnification had 4400, with 20X magnification had 2500, and with 40X magnification had 1600 counts. The x3 CF purification method's sample with a concentration of 0.5 mg/mL and with 10X magnification had 3900, with 20X magnification had 4400, and with 40X magnification had 1950 counts; the sample with a concentration of 0.2 mg/mL and with 10X magnification had 2400, with 20X magnification had 1800, and with 40X magnification had 1650 counts. The 3 DM purification method's sample with a concentration of 0.5 mg/mL and with 10X magnification had 3200, with 20X magnification had 2200, and with 40X magnification had 1600 counts; the sample with a concentration of 0.2 mg/mL and 10X magnification had 3300, with 20X magnification had 3050, and with 40X magnification had 1400 counts.

The fluorescent count results were compared with the same objective lens due to the difference in the optical density of the lenses. Referring to this information, for all of the objective lenses (except for the 20X) and concentrations, the results indicated that the highest fluorescent signal intensity was in the x3 CF & 3 DM purification method. From this result, it can be deduced that the purification effectiveness of this method (in terms of CQD purity) was higher compared to the other purification methods in general. The fluorescent intensity spike in the x3 CF purification method's sample with a concentration of 0.2 mg/mL occurred most likely due to foreign matter contamination as there was a major salt presence within the structure other than the CQDs (see Fig. 13).

The Zeta potential analysis results of the CQDs showed that all CQDs had negative surface charge, independent from the purification method (Fig. 14A). The surface charge decreased significantly for all purification methods as the concentration increased from 0.2 mg/mL to 3 mg/mL, however, not much of a difference was observed between samples that had the same concentration but different purification methods (Fig. 14A). When the surface charges of the samples that have the same concentrations but different purification methods were analyzed statistically by using the two-way ANOVA test (Tukey's test), it was found that x3 CF and 3 DM samples alongside 3 DM and x3 CF & 3 DM samples were statistically significant for both concentrations whereas x3 CF and x3 CF & 3 DM samples were statistically insignificant (Fig. B.20). The negative surface charge of the CQDs may arise from the carboxyl group which was supported by the FT-IR results (Fig. 14B). It is known that negatively charged nanomaterials are taken up less by the cell, and remain in the bloodstream longer but are assimilated better when compared to positively charged nanomaterials [67]. Also, these negatively charged materials are more evenly distributed among cells when taken up from them compared to positively charged materials at nanoscale [67]. CQDs having negative surface charge are known to

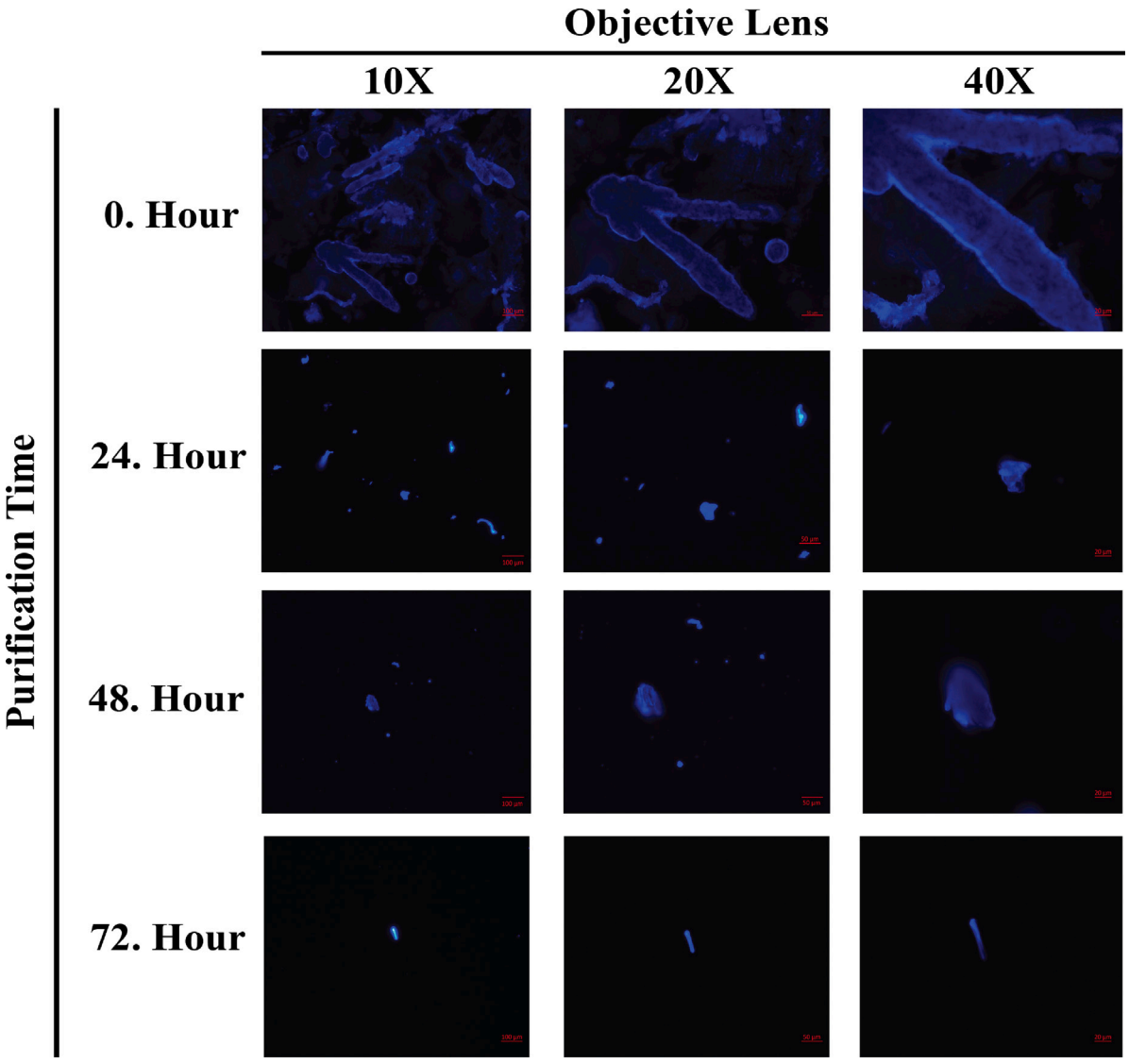


Fig. 8. Fluorescent images of the samples taken from the membrane tubing at 0 h, 24 h, 48 h, and 72 h for 10X, 20X, and 40X objective lenses.

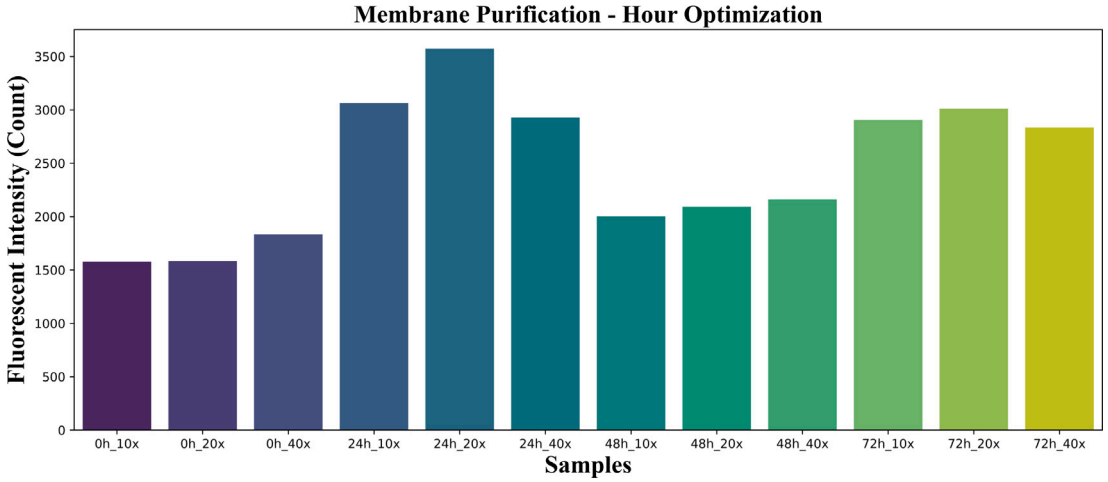


Fig. 9. Fluorescent intensities of the images displayed in Fig. 8.

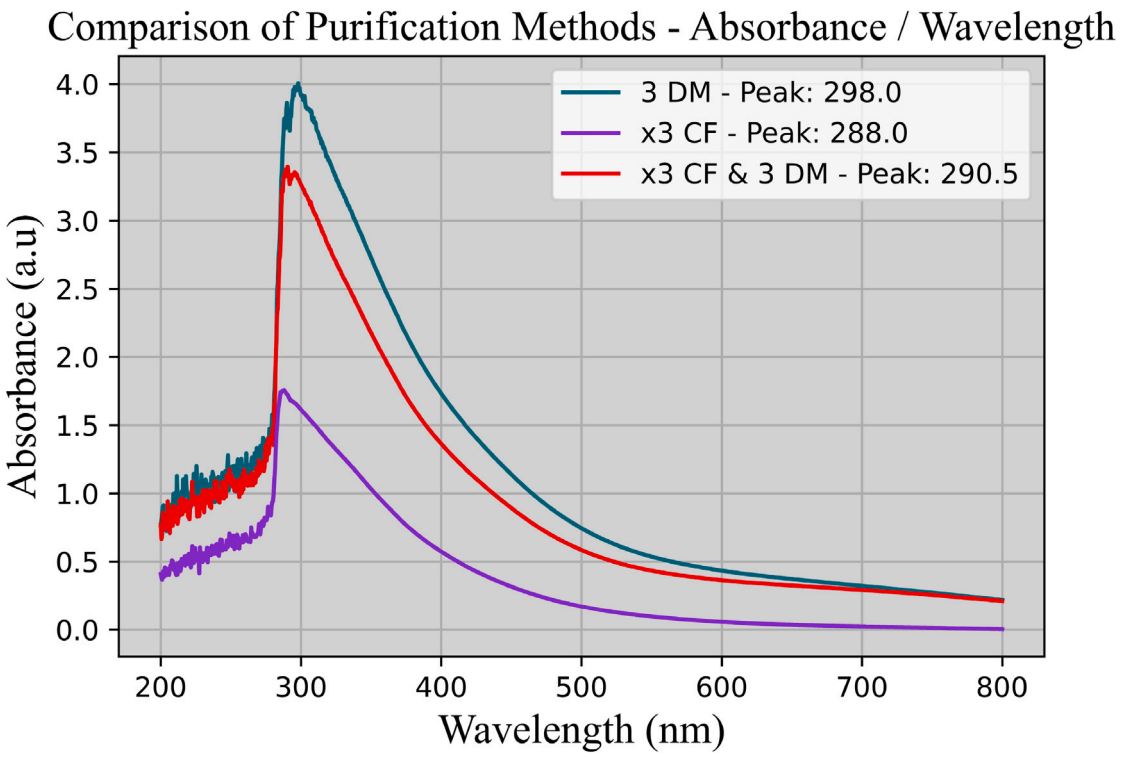


Fig. 10. Absorbance analysis of CQDs with the concentration of 200 μg/mL by the UV–VIS spectrophotometer. x3 CF: 3 times centrifugation, 3 DM: 3 days membrane tubing (MWCO: 1 kDa), x3 CF & 3 DM: 3 times centrifugation & 3 days membrane tubing (MWCO: 1 kDa).

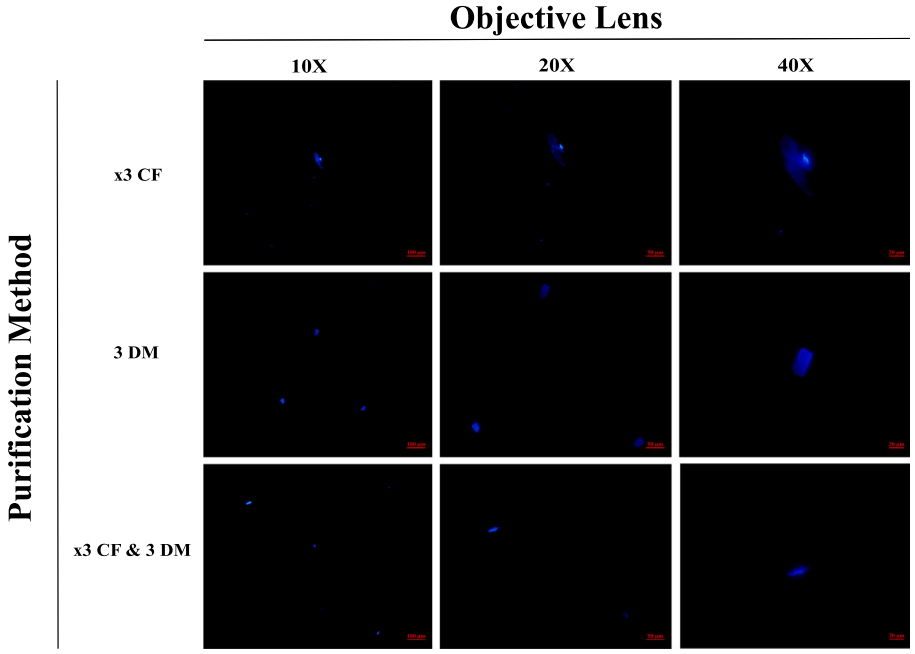


Fig. 11. CQD fluorescence microscopy images that have 200 μg/mL (0.2 mg/mL) concentration, with different purification methods, and with excitation of 365 nm wavelength. 10X scale bar: 100 μm, 20X scale bar: 50 μm, 40X scale bar: 20 μm.

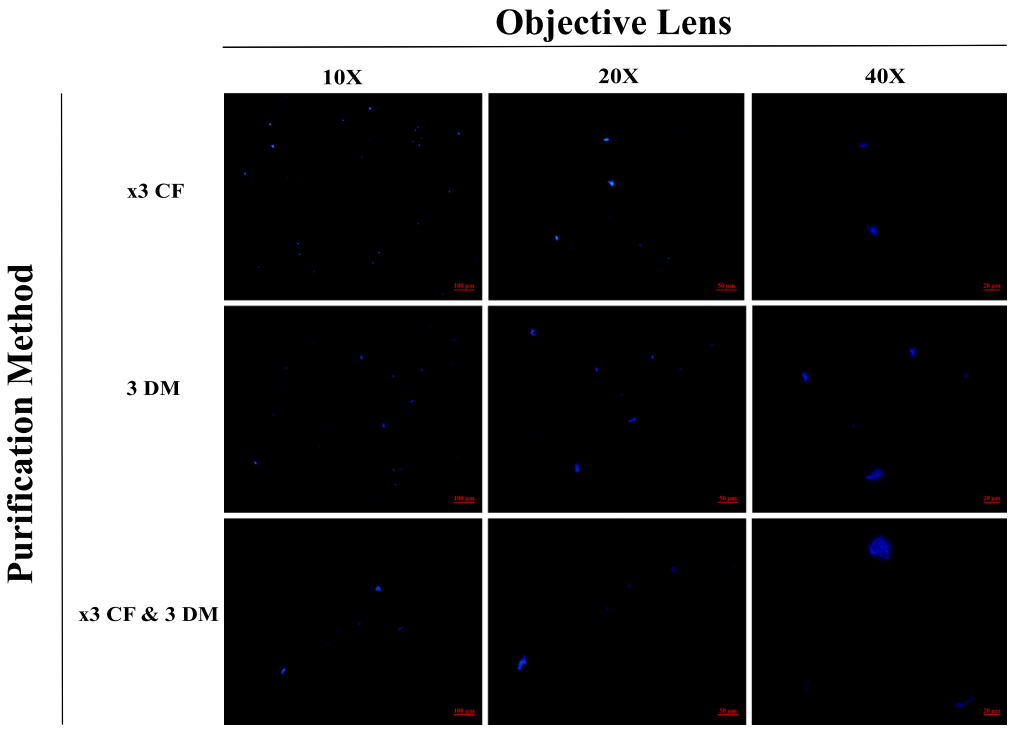


Fig. 12. CQD fluorescence microscopy images that have 500 μg/mL (0.5 mg/mL) concentration, with different purification methods, and with excitation of 365 nm wavelength. 10X scale bar: 100 μm, 20X scale bar: 50 μm, 40X scale bar: 20 μm.

increase the efficiency of the drug delivery to the tumors or cancer cells in their usage as theranostic nanoparticles with chemotherapeutic drugs since positively charged chemotherapeutic drugs bind to negatively charged CQDs more effectively with electrostatic interactions [20,67,68]. Due to this fact, it is thought that CQDs produced in the study can have anticancer effects, and this can be investigated in future studies.

In the FT-IR analysis, it was indicated that the purification method did not change the surface groups of the CQDs since the peaks that correspond to the same bonds were observed for all the purification methods (Fig. 14B, Fig. C.21). Even though the peak wavenumber did not change depending on the purification approach, differences in transmittance % were observed (Fig. 14B). In the sample purified by x3 CF & 3 DM method, especially the peaks representing the C-O aliphatic ether bond (1170 cm^{-1}) and the C-H or C-O bending bond (1038 cm^{-1}) had relatively deep transmittance % compared to other two samples (Fig. 14B). In the sample purified by x3 CF & 3 DM method the peaks at the wavenumber 3409, 2925, 1446, 1170, 1038 cm^{-1} correspond to O-H, C-H, C-O-C, C-O, C-H/C-O bonds at the surface of the CQDs, respectively [65].

It was observed that the hydrodynamic radius of the CQDs changed in both concentrations (0.2 mg/mL and 0.5 mg/mL) for all the purification methods (Fig. 15). For the samples that had 0.5 mg/mL concentration, the smallest hydrodynamic radius was obtained with the 3 DM purification method, meanwhile, the biggest hydrodynamic radius was obtained with the x3 CF method (Fig. 15). For the samples that had 0.2 mg/mL concentration, the smallest hydrodynamic radius was obtained with the x3 CF & 3 DM purification method, meanwhile, the biggest hydrodynamic radius was obtained with the x3 CF method (Fig. 15). Since the biggest hydrodynamic radii were obtained with the x3 CF purification method, it is thought that centrifugation increases the aggregation of CQDs in water. As mentioned before, the hydrodynamic radius might big even though the concentration of CQDs is low, which might be due to the fact that less concentrated CQDs in water interact polarly more with the water molecules compared to the highly concentrated CQDs in water [56,57].

To obtain the elemental compositions and morphologies of CQDs purified with different purification methods, EDS, SEM, and TEM analyses were made. The EDS analysis results (Fig. 16) show the average percentage of elements that were present in the CQDs obtained by 3 different measurements for each purification method given in Table 3. If the sulfur and sodium were to be considered as impurities, the x3 CF & 3 DM, 3 DM, and x3 CF purification methods would have 3.1%, 8.8%, and 16.3% of impurity. From the EDS results, it can be deduced that the x3 CF & 3 DM purification method purifies the samples the most when compared to the x3 CF and 3 DM purification methods.

In the SEM images of samples with different purification methods (Fig. 17), it was observed that the CQDs had similar and spherical morphologies independent from the purification method. Furthermore, the signal received from the SEM image of x3 CF & 3 DM sample had a greater magnitude than the signals of the other samples. It is thought that due to having more impurities, as shown in Fig. 16, the back-scattered electrons might not have been picked up by the detectors of the SEM, resulting in the signal decrease in the SEM image of the sample with x3 CF and 3 DM purification method. It was also noted that due to impurities such as sodium and sulfate, the surfaces of x3 CF and 3 DM purification method samples were mostly covered with salt.

As can be seen in the TEM images of samples with different purification methods, it was observed that the morphologies of CQDs were spherical, but in these images, there were mostly clusters of CQDs seen rather than individual CQDs (Fig. 18). For instance, in the TEM image of the x3 CF & 3 DM purification method's sample, mostly clusters were observed. On the other hand, in the TEM images of the x3 CF purification method's sample, individual CQDs were encountered. The observation of clusters could likely be due to aggregation over time as the acquisition of TEM images took longer than it was anticipated.

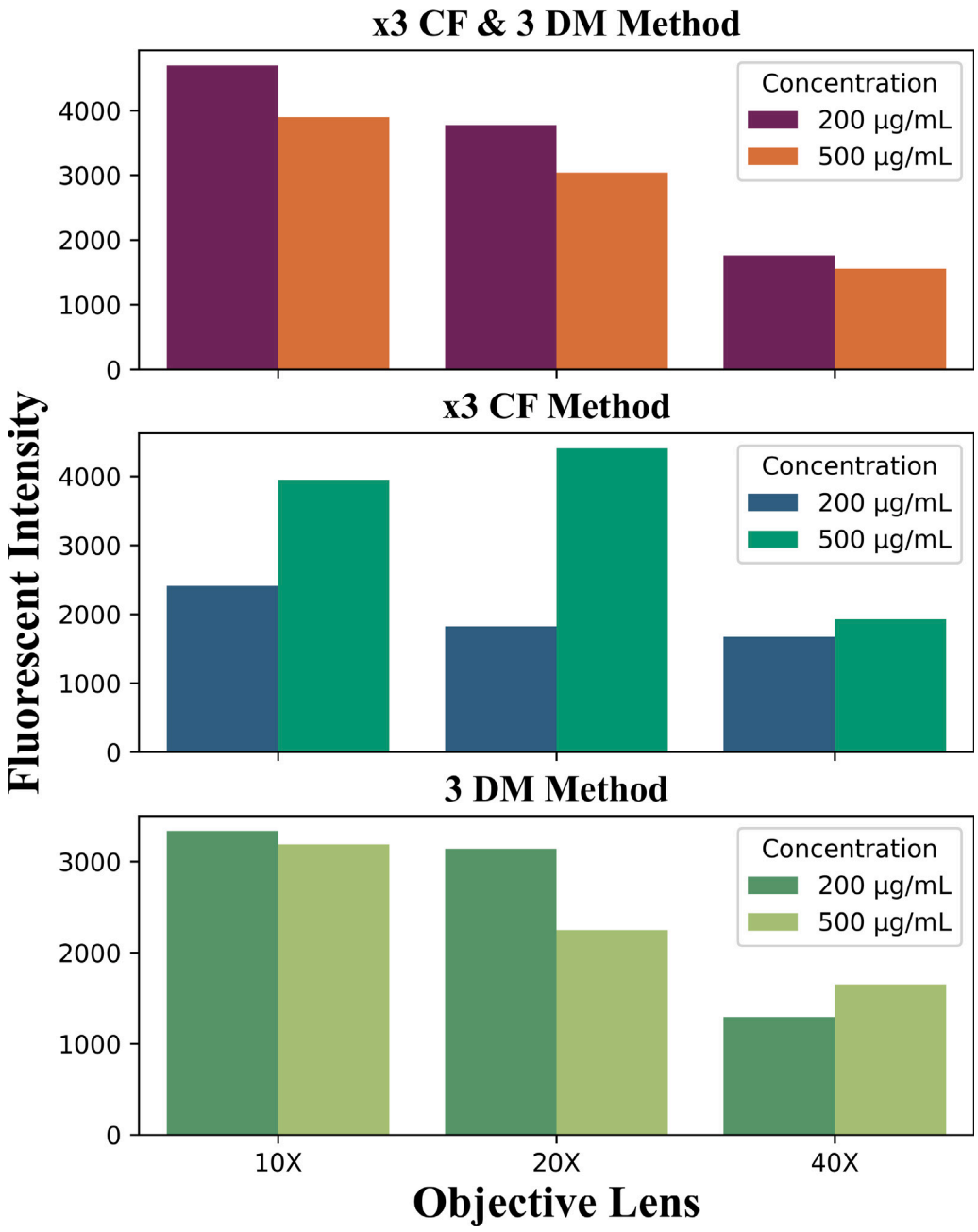


Fig. 13. Image analysis of fluorescence images that were given in Figs. 11 and 12. The figures were separated by the utilized purification method, as indicated by their titles. Each figure's *y*-axis contains the fluorescent intensity in terms of the average count which was calculated from their respective fluorescent image.

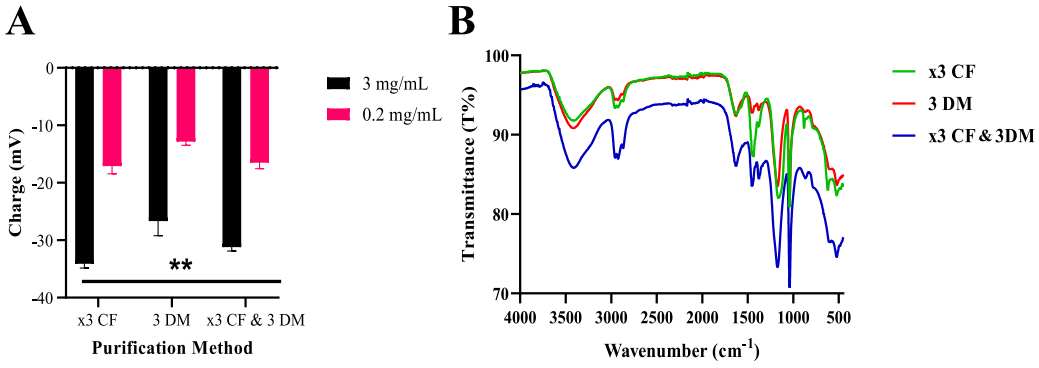


Fig. 14. CQD Zeta Potential & FT-IR Analysis Based on Purification Method. A: Zeta potential analysis, B: A: FT-IR analysis. x3 CF: 3 times centrifugation, 3 DM: 3 days membrane tubing (MWCO: 1 kDa), x3 CF & 3 DM: 3 times centrifugation & 3 days membrane tubing (MWCO: 1 kDa). (ns:non-significant, *p < 0.05, **p < 0.01, ***p < 0.001).

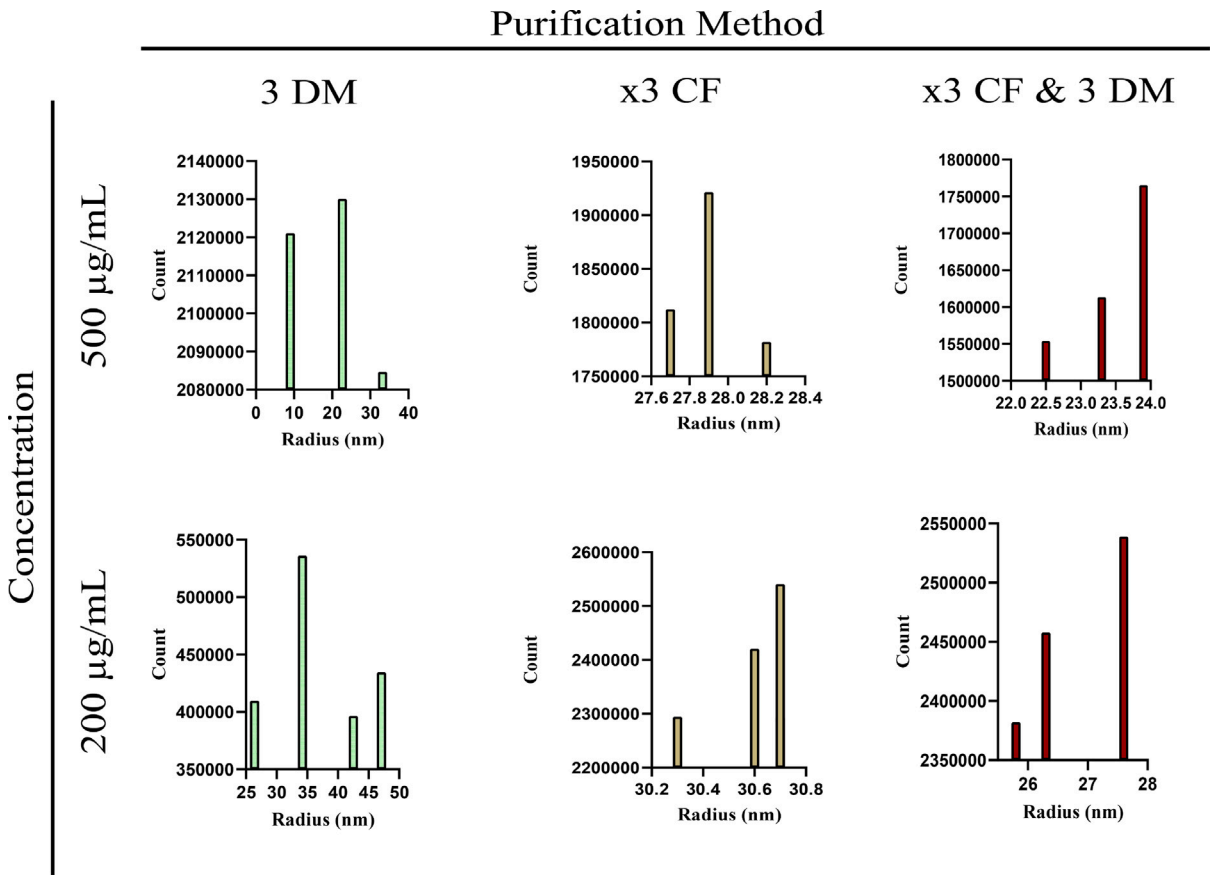


Fig. 15. Hydrodynamic radii of CQDs with concentrations of 200 and 500 µg/mL (0.2 and 0.5 mg/mL) which have different purification methods. (x3 CF: 3 times centrifugation (6000 rpm, 15 min); 3 DM: dialysis membrane (MWCO: 1 kDa) tubing for 3 days; x3 CF & 3 DM: centrifugation 3 times (6000 rpm, 15 min) & dialysis membrane (MWCO: 1 kDa) tubing for 3 days).

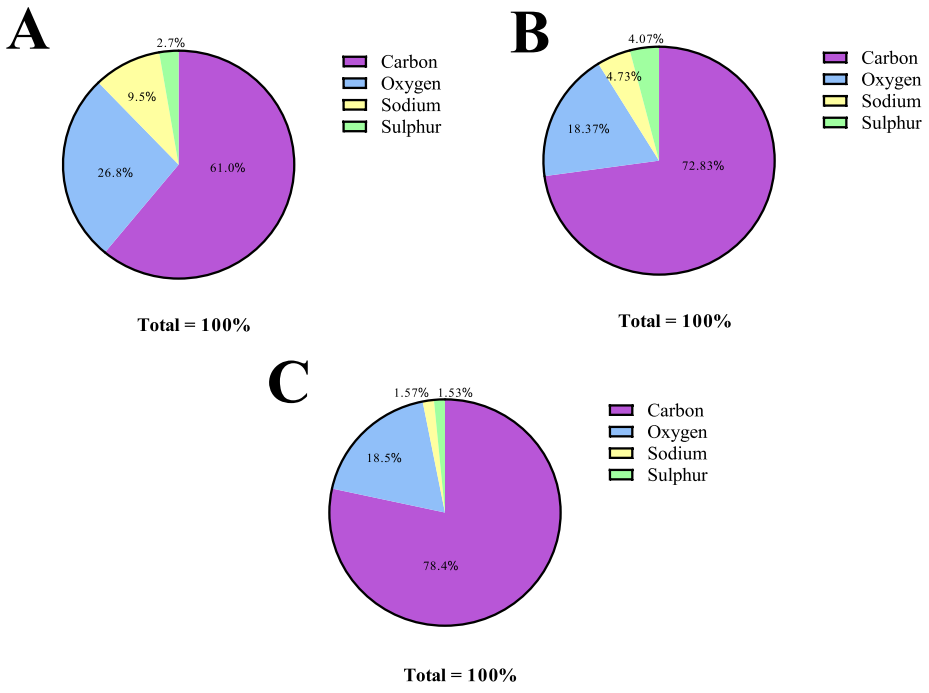


Fig. 16. Purification Method Elemental Composition Analysis done by EDS. The atomic% data shown here, are the averages of the atomic% data presented in Table 3. A: CQD purified by 3 times centrifugation, B: CQD purified by dialysis membrane tubing (MWCO: 1 kDa) for 3 days, C: CQD purified by centrifugation 3 times and dialysis membrane tubing (MWCO: 1 kDa) for 3 days. Scale Bar: 500 nm.

Table 3
Elemental composition results with their standard deviation values obtained by EDS analysis of CQDs with different purification methods.

Purification method	Atomic % Carbon	Atomic % Oxygen	Atomic % Sodium	Atomic % Sulfur
Centrifugation 3 times	72.4 ± 0.076	21.2 ± 0.122	4.9 ± 0.082	1.6 ± 0.045
Centrifugation 3 times	37.8 ± 0.105	39.3 ± 0.090	18.3 ± 0.070	4.6 ± 0.034
Centrifugation 3 times	72.8 ± 0.076	19.9 ± 0.115	5.3 ± 0.074	1.9 ± 0.031
Dialysis membrane tubing for 3 days	73.1 ± 0.083	19.1 ± 0.116	4.6 ± 0.076	3.2 ± 0.026
Dialysis membrane tubing for 3 days	72.9 ± 0.098	16.4 ± 0.127	4.9 ± 0.082	5.7 ± 0.026
Dialysis membrane tubing for 3 days	73.1 ± 0.083	19.1 ± 0.116	4.6 ± 0.076	3.2 ± 0.026
Centrifugation 3 times & dialysis membrane tubing for 3 days	80.8 ± 0.066	16.1 ± 0.135	1.8 ± 0.102	1.3 ± 0.029
Centrifugation 3 times & dialysis membrane tubing for 3 days	76.5 ± 0.069	20.5 ± 0.124	1.4 ± 0.104	1.6 ± 0.036
Centrifugation 3 times & dialysis membrane tubing for 3 days	77.9 ± 0.069	18.9 ± 0.125	1.5 ± 0.100	1.7 ± 0.033

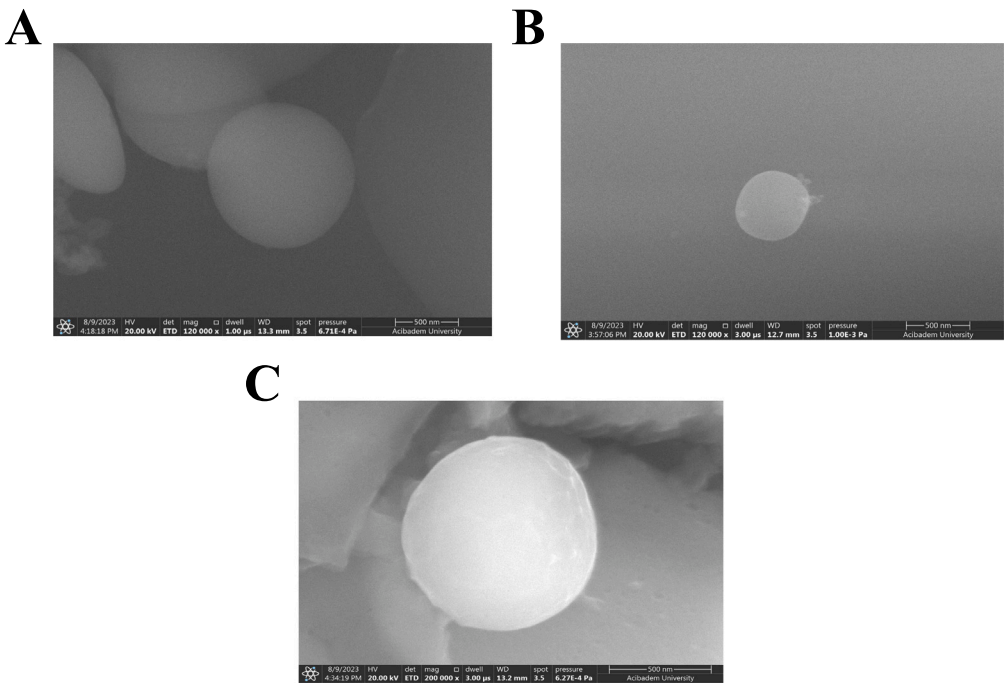


Fig. 17. Morphology of the CQD aggregates with different purification methods obtained by SEM. A: CQD purified by centrifugation of 3 times, B: CQD purified by dialysis membrane tubing (MWCO: 1 kDa) for 3 days, C: CQD purified by centrifugation of 3 times and dialysis membrane tubing (MWCO: 1 kDa) for 3 days. (Scale bar: 500 nm).

However, this clustering of multiple CQDs is a desired property for their application as imaging agents since higher emissions would be detected from the CQD clusters.

In this study, for lowering the particle size, preventing CQD aggregation in an aqueous environment, achieving a more homogeneous size distribution of CQDs, fluorescence spectrometer measurements of CQDs (the excitation and the emission wavelengths of the CQDs), size distribution of isolated CQDs from TEM images, and quantum yield measurement of CQDs were identified as the parts that need improvement. These identified absent and yet-to-be-improved parts are planned to be implemented in future studies to eliminate the lacking parts as much as possible.

The CQDs obtained with this synthesis method are planned to be tested in future studies for their potential as sensors, imaging agents, therapeutic agents, and theranostic agents in biological environments (cancer cells, tumor tissues, animal tissues, etc.) since CQDs are more biocompatible than other QD types. We aim to further pursue *in vitro* and *in vivo* studies and surface modifications with ligand exchanges so that they can be adapted to areas such as targeted drug delivery, photothermal therapy (PTT), and disease diagnosis and treatment [69–71]. In addition, the antimicrobial properties of CQDs produced by this developed method can be examined in the future since CQDs obtained by other methods may show antimicrobial properties [72]. Besides, the CQDs produced with the HBBBS method can have the potential to be used as LEDs when surface modifications are made [73].

4. Conclusions

In this study, for the synthesis of carbon quantum dots (CQDs), sulfuric acid of 98% concentration and pure acetone, which are materials that can be easily found in every laboratory, were mixed in a ratio of 2:1 (sulfuric acid:acetone). The production of CQDs was determined with a definitive indication, a bubble, depending on the dehydration reaction between the sulphuric acid and acetone at high temperatures. In this newly developed synthesis method, the synthesis was conducted in a hot environment (140-165 °C) and therefore, the synthesis was

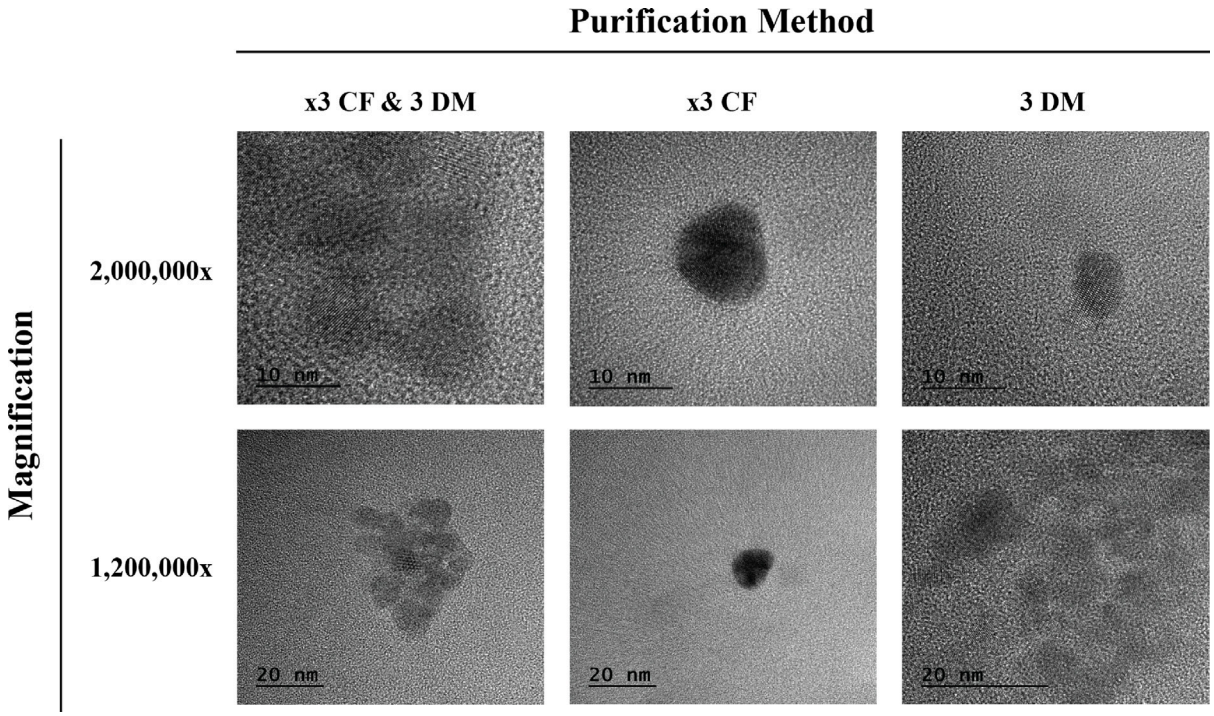


Fig. 18. TEM images of CQD purified with x3 CF & 3 DM, x3 CF, and 3 DM methods with different magnifications. (Scale bar: 10 nm and 20 nm for 2,000,000x and 1,200,000x respectively).

named as the hot bubble synthesis (HBBBS) method. In the developed method, it was found that removing the mixture from the hot environment 30–60 s after the bubbles completely covered the surface of the mixture was the most optimum incubation time. In addition, the purification method optimization was made for the developed synthesis method, and it was determined that the purest CQDs were obtained with the x3 CF & 3 DM purification method. The CQDs obtained by the developed synthesis and purification method showed characteristic properties, therefore, in future studies, their use as *in vitro* and *in vivo* bioimaging agents, biosensors, or theranostic nanoparticles on a specific region (organ, tumor tissue, etc.) can be examined by targeting the specific region by performing surface modifications.

5. Patents

A patent application has been submitted to the TR Patent Office (TÜRKPATENT).

Funding

This research was funded by Acibadem University BAP Coordination Unit grant number 71.

CRediT authorship contribution statement

Beste Dipcin: Writing – review & editing, Writing – original draft, Project administration, Methodology, Investigation, Data curation, Conceptualization. **Bora Guvendiren:** Writing – review & editing, Writing – original draft, Methodology, Investigation, Data curation, Conceptualization. **Selcuk Birdogan:** Writing – original draft, Data curation, Conceptualization. **Bukem Tanoren:** Writing – review & editing, Writing – original draft, Validation, Supervision, Project administration, Methodology, Data curation, Conceptualization.

Declaration of competing interest

The authors declare that they have no known competing financial interests or personal relationships that could have appeared to influence the work reported in this paper.

Acknowledgments

We would like to thank Gokcen Ozgun for her help with SEM imaging and EDS analysis, and Ozgul Gok Ozatay and Kadriye Kizilbey for their consultancy. Also, we would like to thank Dogan Akcan and Bahcesehir University for PL analysis. The authors thank all the volunteers who contributed to this project.

Appendix A. Material characteristics that was taken at 150 °C

See Fig. A.19.

Appendix B. Two-way Anova

See Fig. B.20.

Appendix C. Purification method FT-IR

See Fig. C.21.

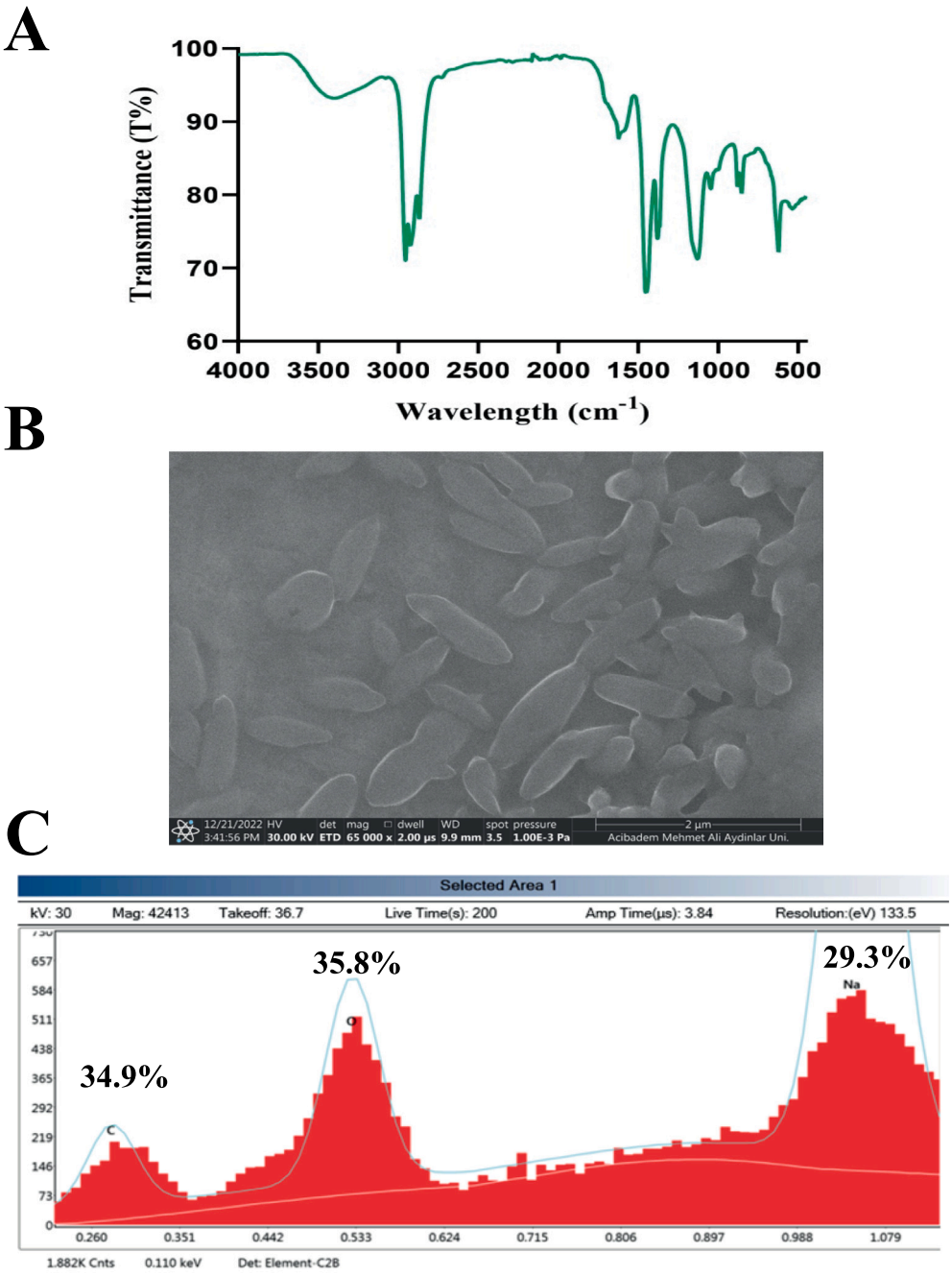


Fig. A.19. The characteristic results of the material that was taken when the reaction turned black approximately at 150 °C. The material was purified by 3 times centrifugation. A: FT-IR result, B: SEM image, C: EDS analysis result, the atomic weight percentages (%) of the elements were presented in the figure for carbon (C), oxygen (O), and sodium (Na) elements, respectively.

Tukey's multiple comparisons test	Mean Diff.	95.00% CI of diff.	Significant?	Summary	Adjusted P Value
3 mg/mL					
x3 SF vs. 3 GM	-7.433	-10.33 to -4.536	Yes	****	<0.0001
x3 SF vs. x3 SF & 3 GM	-2.867	-5.764 to 0.03092	No	ns	0.0526
3 GM vs. x3 SF & 3 GM	4.567	1.669 to 7.464	Yes	**	0.0032
0.2 mg/mL					
x3 SF vs. 3 GM	-4.300	-7.198 to -1.402	Yes	**	0.0050
x3 SF vs. x3 SF & 3 GM	-0.6000	-3.498 to 2.298	No	ns	0.8472
3 GM vs. x3 SF & 3 GM	3.700	0.8024 to 6.598	Yes	*	0.0134

Fig. B.20. The results of two-way ANOVA Tukey's test between the surface charges of CQDs with different purification methods. x3 CF: purified by centrifugation 3 times (6000 rpm, 15 min), 3 DM: Purified by dialysis membrane tubing (MWCO: 1 kDa) for 3 days, x3 CF & 3 DM: Purified by centrifugation 3 times (6000 rpm, 15 min) followed by dialysis membrane tubing (MWCO: 1 kDa) for 3 days. [ns: non-significant (statistically not significant) $^{*}p < 0.05$, $^{**}p < 0.01$, $^{***}p < 0.001$].

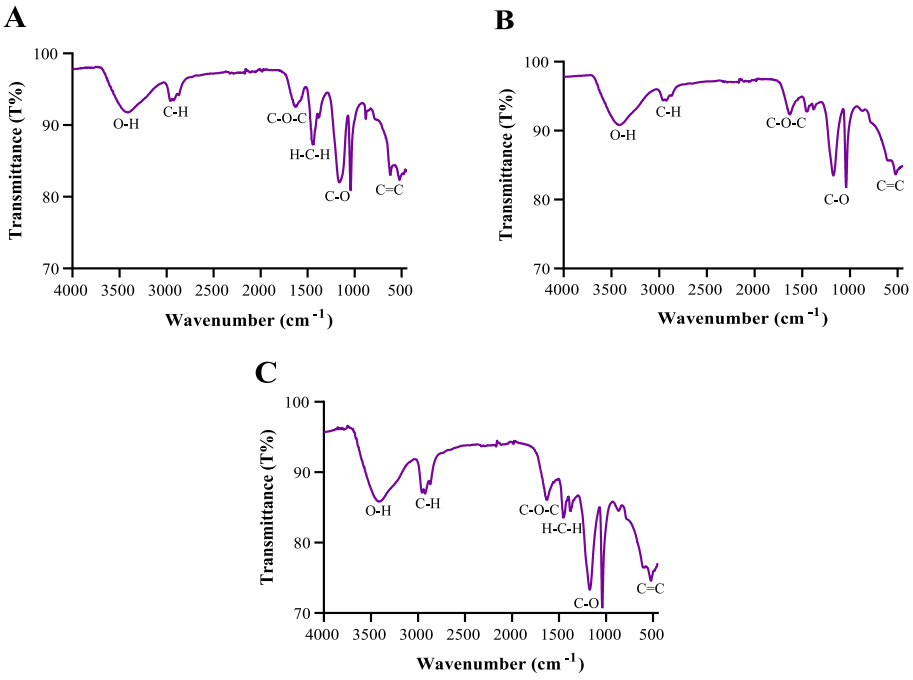


Fig. C.21. Chemical bonds on the CQD's surface obtained by FT-IR analysis that were purified by different purification methods. A: CQDs purified by 3 times centrifugation (6000 rpm, 15 min), B: CQDs purified dialysis membrane tubing (MWCO: 1 kDa) for 3 days, C: Centrifugation 3 times (6000 rpm, 15 min) followed by dialysis membrane tubing (MWCO: 1 kDa) for 3 days.

Data availability

The data presented in the manuscript will be available upon request.

References

[1] C.T. Matea, T. Mocan, F. Tabaran, T. Pop, O. Mosteanu, C. Puia, C. Iancu, L. Mocan, Quantum dots in imaging, drug delivery and sensor applications, Int. J. Nanomedicine 12 (2017) 5421, http://dx.doi.org/10.2147/IJN.S138624.

[2] B.T. Bilen, M. Parlak, M.B. Unlu, Scanning acoustic microscopy of quantum dot aggregates, Biomed. Phys. Eng. Express 5 (2019) 065025, http://dx.doi.org/10.1088/2057-1976/ab519a.

[3] J. Weng, X. Song, L. Li, H. Qian, K. Chen, X. Xu, C. Cao, J. Ren, Highly luminescent CdTe quantum dots prepared in aqueous phase as an alternative fluorescent probe for cell imaging, Talanta 70 (2) (2006) 397–402, http://dx.doi.org/10.1016/j.talanta.2006.02.064.

[4] C. Maksoudian, S.J. Soenen, K. Susumu, E. Oh, I.L. Medintz, B.B. Manshian, A multiparametric evaluation of quantum dot size and surface-grafted peptide density on cellular uptake and cytotoxicity, Bioconjug. Chem. 31 (4) (2020) 1077–1087, http://dx.doi.org/10.1021/acs.bioconjchem.0c00078.

[5] O.D. Neikov, N.A. Yefimov, Chapter 9 - nanopowders, in: O.D. Neikov, S.S. Naboychenko, N.A. Yefimov (Eds.), Handbook of Non-Ferrous Metal Powders, second ed., Elsevier, Oxford, 2019, pp. 271–311, http://dx.doi.org/10.1016/B978-0-08-100543-9.00009-9, URL https://www.sciencedirect.com/science/article/pii/B9780081005439000099.

[6] S. Dhara, A. Arora, S. Bera, J. Ghatak, Multiphonon probe in ZnS quantum dots, J. Raman Spectrosc. 41 (10) (2010) 1102–1105.

[7] F. Divsar, Quantum dots: Fundamental and applications, IntechOpen, 2020, URL https://books.google.com.tr/books?id=jEv9DwAAQBAJ.

[8] P.N. Joshi, S. Kundu, S.K. Sanghi, D. Sarkar, Graphene quantum dots-from emergence to nanotheranostic applications, Smart Drug Deliv. Syst. 7 (2016) 159–195.

[9] P. Ramasamy, N. Kim, Y.-S. Kang, O. Ramirez, J.-S. Lee, Tunable, bright, and narrow-band luminescence from colloidal indium phosphide quantum dots, Chem. Mater. 29 (16) (2017) 6893–6899, http://dx.doi.org/10.1021/acs.chemmater.7b02204.

[10] K.J. McHugh, L. Jing, A.M. Behrens, S. Jayawardena, W. Tang, M. Gao, R. Langer, A. Jaklenec, Biocompatible semiconductor quantum dots as cancer imaging agents, Adv. Mater. 30 (18) (2018) 1706356, http://dx.doi.org/10.1002/adma.201706356.

[11] P. Kamble, D. Malavekar, A.P. Tiwari, Natural biowaste derived fluorescent carbon quantum dots: Synthesis, characterization and biocompatibility study, J. Fluorescence 34 (1) (2024) 191–201, http://dx.doi.org/10.1007/s10895-023-03244-w.

[12] N. Arsalani, P. Nezhad-Mokhtari, E. Jabbari, Microwave-assisted and one-step synthesis of PEG passivated fluorescent carbon dots from gelatin as an efficient nanocarrier for methotrexate delivery, Artif. Cells Nanomedicine Biotechnol. 47 (1) (2019) 540–547, http://dx.doi.org/10.1080/21691401.2018.1562460.

[13] Y. Wang, A. Hu, Carbon quantum dots: synthesis, properties and applications, J. Mater. Chem. C 2 (34) (2014) 6921–6939, http://dx.doi.org/10.1039/C4TC00988F.

[14] V. Singh, S. Kashyap, U. Yadav, A. Srivastava, A.V. Singh, R.K. Singh, S.K. Singh, P.S. Saxena, Nitrogen doped carbon quantum dots demonstrate no toxicity under in vitro conditions in a cervical cell line and in vivo in swiss albino mice, Toxicol. Res. 8 (3) (2019) 395–406, http://dx.doi.org/10.1039/c8tx00260f.

[15] S. Pandey, M. Thakur, A. Mewada, D. Anjarlekar, N. Mishra, M. Sharon, Carbon dots functionalized gold nanorod mediated delivery of doxorubicin: tri-functional nano-worms for drug delivery, photothermal therapy and bioimaging, J. Mater. Chem. B 1 (38) (2013) 4972–4982, http://dx.doi.org/10.1039/C3TB20761G.

[16] Y. Wu, C. Li, H.C. van der Mei, H.J. Busscher, Y. Ren, Carbon quantum dots derived from different carbon sources for antibacterial applications, Antibiotics 10 (6) (2021) 623, http://dx.doi.org/10.3390/antibiotics10060623.

[17] T. Yuan, T. Meng, P. He, Y. Shi, Y. Li, X. Li, L. Fan, S. Yang, Carbon quantum dots: an emerging material for optoelectronic applications, J. Mater. Chem. C 7 (23) (2019) 6820–6835, http://dx.doi.org/10.1039/C9TC01730E.

[18] N. Azam, M. Najabat Ali, T. Javaid Khan, Carbon quantum dots for biomedical applications: review and analysis, Front. Mater. 8 (2021) 700403, http://dx.doi.org/10.3389/fmats.2021.700403.

[19] F. Yuan, T. Yuan, L. Sui, Z. Wang, Z. Xi, Y. Li, X. Li, L. Fan, Z. Tan, A. Chen, et al., Engineering triangular carbon quantum dots with unprecedented narrow bandwidth emission for multicolored LEDs, Nat. Commun. 9 (1) (2018) 2249, http://dx.doi.org/10.1038/s41467-018-04635-5.

[20] K. Soumya, N. More, M. Choppadandi, D. Aishwarya, G. Singh, G. Kapusetti, A comprehensive review on carbon quantum dots as an effective photosensitizer and drug delivery system for cancer treatment, Biomed. Technol. 4 (2023) 11–20, http://dx.doi.org/10.1016/j.bmt.2023.01.005.

[21] S. Miao, K. Liang, B. Kong, Förster resonance energy transfer (FRET) paired carbon dot-based complex nanoprobes: versatile platforms for sensing and imaging applications, Mater. Chem. Front. 4 (1) (2020) 128–139, http://dx.doi.org/10.1039/c9qm00538b.

[22] F. Du, Y. Min, F. Zeng, C. Yu, S. Wu, A targeted and FRET-based ratiometric fluorescent nanoprobe for imaging mitochondrial hydrogen peroxide in living cells, Small 10 (5) (2014) 964–972, http://dx.doi.org/10.1002/smll.201302036.

[23] A. Vibhute, T. Patil, R. Gambhir, A.P. Tiwari, Fluorescent carbon quantum dots: Synthesis methods, functionalization and biomedical applications, Appl. Surf. Sci. Adv. 11 (2022) 100311, http://dx.doi.org/10.1016/j.apsadv.2022.100311.

[24] X. Chen, S. Zhao, X. Kang, C. He, P. Zhao, X. Meng, A.J. Ragauskas, J. Pang, X. Song, Gradient synthesis of carbon quantum dots and activated carbon from pulp black liquor for photocatalytic hydrogen evolution and supercapacitor, Adv. Compos. Hybrid Mater. 6 (4) (2023) 131, http://dx.doi.org/10.1007/s42114-023-00714-4.

[25] P.K. Yadav, S. Chandra, V. Kumar, D. Kumar, S.H. Hasan, Carbon quantum dots: synthesis, structure, properties, and catalytic applications for organic synthesis, Catalysts 13 (2) (2023) 422, http://dx.doi.org/10.3390/catal13020422.

[26] X. Guan, Z. Li, X. Geng, Z. Lei, A. Karakoti, T. Wu, P. Kumar, J. Yi, A. Vinu, Emerging trends of carbon-based quantum dots: Nanoarchitectonics and applications, Small 19 (17) (2023) 2207181, http://dx.doi.org/10.1002/smll.202207181.

[27] F. Chao-Mujica, L. Garcia-Hernández, S. Camacho-López, M. Camacho-López, M. Camacho-López, D. Reyes Contreras, et al., Carbon quantum dots by submerged arc discharge in water: Synthesis, characterization, and mechanism of formation, J. Appl. Phys. 129 (16) (2021) http://dx.doi.org/10.1063/5.0040322.

[28] A. Kaczmarek, J. Hoffman, J. Morgiel, T. Mościcki, L. Stobiński, Z. Szymański, A. Małolepszy, Luminescent carbon dots synthesized by the laser ablation of graphite in polyethylenimine and ethylenediamine, Materials 14 (4) (2021) 729, http://dx.doi.org/10.3390/ma14040729.

[29] Q. Wang, C. Zhang, G. Shen, H. Liu, H. Fu, D. Cui, Fluorescent carbon dots as an efficient siRNA nanocarrier for its interference therapy in gastric cancer cells, J. Nanobiotechnol. 12 (1) (2014) 1–12, http://dx.doi.org/10.1186/s12951-014-0058-0.

[30] S. Shishodia, V. Rimal, P. Srivastava, Synthesis of tunable high-thermal stability carbon dots via functionalization for applications in high-temperature environment, Appl. Nanosci. 11 (2021) 1691–1706, http://dx.doi.org/10.1007/s13204-021-01814-7.

[31] S.-R. Zhang, S.-K. Cai, G.-Q. Wang, J.-Z. Cui, C.-Z. Gao, One-step synthesis of n, P-doped carbon quantum dots for selective and sensitive detection of Fe2+ and Fe3+ and scale inhibition, J. Mol. Struct. 1246 (2021) 131173, http://dx.doi.org/10.1016/j.molstruc.2021.131173.

[32] M.P. Romero, F. Alves, M.D. Stringasci, H.H. Buzzá, H. Ciol, N.M. Inada, V.S. Bagnato, One-pot microwave-assisted synthesis of carbon dots and in vivo and in vitro antimicrobial photodynamic applications, Front. Microbiol. 12 (2021) 662149, http://dx.doi.org/10.3389/fmicb.2021.662149.

[33] H. Eskalen, S. Uruş, S. Cömertpay, A.H. Kurt, Ş. Özgan, Microwave-assisted ultra-fast synthesis of carbon quantum dots from linter: Fluorescence cancer imaging and human cell growth inhibition properties, Ind. Crop. Prod. 147 (2020) 112209, http://dx.doi.org/10.1016/j.indcrop.2020.112209.

[34] Y. Hu, Z. Gao, Hot-injection strategy for 1-min synthesis of carbon dots from oxygen-containing organic solvents: Toward fluorescence sensing of hemoglobin, Dye. Pigment. 165 (2019) 429–435, http://dx.doi.org/10.1016/j.dyepig.2019.03.001.

[35] I. Singh, R. Arora, H. Dhiman, R. Pahwa, Carbon quantum dots: Synthesis, characterization and biomedical applications, Turk. J. Pharm. Sci 15 (2) (2018) 219–230, http://dx.doi.org/10.4274/tjps.63497.

[36] S. Chai, L. Zhou, S. Pei, Z. Zhu, B. Chen, P-doped carbon quantum dots with antibacterial activity, Micromachines 12 (9) (2021) 1116, http://dx.doi.org/10.3390/mi12091116.

[37] C.-Y. Chen, Y.-H. Tsai, C.-W. Chang, Evaluation of the dialysis time required for carbon dots by HPLC and the properties of carbon dots after HPLC fractionation, New J. Chem. 43 (16) (2019) 6153–6159, http://dx.doi.org/10.1039/c9nj00434c.

[38] S.M. Kane, R.S. Timonen, M.-T. Leu, Heterogeneous chemistry of acetone in sulfuric acid solutions: implications for the upper troposphere, J. Phys. Chem. A 103 (46) (1999) 9259–9265, http://dx.doi.org/10.1021/jp9926692.

[39] H. Wang, Z. Jiang, Y. Wang, S. Sanvito, S. Hou, Quantitative interpretation of the low-bias conductance of au–mesitylene–au molecular junctions formed from mesitylene monolayers, ChemPhysChem 17 (14) (2016) 2272–2277, http://dx.doi.org/10.1002/cphc.201600264.

[40] Ø. Borck, E. Schröder, Methylbenzenes on graphene, Surf. Sci. 664 (2017) 162–167, http://dx.doi.org/10.1016/j.susc.2017.06.012.

[41] S.-C. Qi, Y. Liu, A.-Z. Peng, D.-M. Xue, X. Liu, X.-Q. Liu, L.-B. Sun, Fabrication of porous carbons from mesitylene for highly efficient CO2 capture: A rational choice improving the carbon loop, Chem. Eng. J. 361 (2019) 945–952, http://dx.doi.org/10.1016/j.cej.2018.12.167.

[42] W. Zhang, Nanoparticle aggregation: principles and modeling, Nanomater. Impacts Cell Biol. Med. (2014) 19–43.

[43] I. Gosens, J.A. Post, L.J. de la Fonteyne, E.H. Jansen, J.W. Geus, F.R. Cassee, W.H. de Jong, Impact of agglomeration state of nano-and submicron sized gold particles on pulmonary inflammation, Part. Fibre Toxicol. 7 (2010) 1–11.

[44] N. Ngafwan, H. Rasyid, E.S. Abood, W.K. Abdelbasset, S.G. Al-Shawi, D. Bokov, A.T. Jalil, Study on novel fluorescent carbon nanomaterials in food analysis, Food Sci. Technol. 42 (2021) e37821, http://dx.doi.org/10.1590/fst.37821.

[45] S. Das, S. Mondal, D. Ghosh, Carbon quantum dots in bioimaging and biomedicines, Front. Bioeng. Biotechnol. 11 (2023) http://dx.doi.org/10.3389/fbioe.2023.1333752.

[46] S. Dua, P. Kumar, B. Pani, A. Kaur, M. Khanna, G. Bhatt, Stability of carbon quantum dots: a critical review, RSC Adv. 13 (20) (2023) 13845–13861, http://dx.doi.org/10.1039/d2ra07180k.

[47] C.S. Yoon, J.M. Ko, M. Latifatu, H.S. Lee, Y.-G. Lee, K.M. Kim, J.H. Won, J. Jo, Y. Jang, J.H. Kim, Electrochemical properties of activated carbon supercapacitor containing sulfonated polypropylene separator coated with a hydrogel polymer electrolyte, Korean Chem. Eng. Res. 52 (5) (2014) 553–557, http://dx.doi.org/10.9713/kcer.2014.52.5.553.

[48] M. Razeghi, The Mystery of Carbon: An Introduction to Carbon Materials, IOP Publishing, 2019, http://dx.doi.org/10.1088/2053-2563/ab35d1ch1.

[49] S.N. Baker, G.A. Baker, Luminescent carbon nanodots: emergent nanolights, Angew. Chem., Int. Ed. 49 (38) (2010) 6726–6744, http://dx.doi.org/10.1002/anie.200906623.

[50] S. Zhu, Y. Song, X. Zhao, J. Shao, J. Zhang, B. Yang, The photoluminescence mechanism in carbon dots (graphene quantum dots, carbon nanodots, and polymer dots): current state and future perspective, Nano Res. 8 (2015) 355–381, http://dx.doi.org/10.1007/s12274-014-0644-3.

[51] W. Fawaz, J. Hasian, I. Alghoraibi, Synthesis and physicochemical characterization of carbon quantum dots produced from folic acid, Sci. Rep. 13 (1) (2023) 18641.

[52] B. Rooj, U. Mandal, A review on characterization of carbon quantum dots, Vietnam J. Chem. 61 (6) (2023) 693–718.

[53] S. Das, What are the reasons behind getting a blue shift and a red shift in the same photo luminescence spectrum? 2018.

[54] P. Kumar, S. Dua, R. Kaur, M. Kumar, G. Bhatt, Correction: A review on advancements in carbon quantum dots and their application in photovoltaics, RSC Adv. 12 (11) (2022) 6432, http://dx.doi.org/10.1039/d2ra90018a.

[55] S.K. Filippov, R. Khusnutdinov, A. Murmiliuk, W. Inam, L.Y. Zakharova, H. Zhang, V.V. Khutoryanskiy, Dynamic light scattering and transmission electron microscopy in drug delivery: a roadmap for correct characterization of nanoparticles and interpretation of results, Mater. Horiz. 10 (12) (2023) 5354–5370, http://dx.doi.org/10.1039/d3mh00717k.

[56] M. Zhao, M. Taani, J. Cole, B. Crudele, B. Zou, N. Bhuiyan, E. Chowdhury, Y. Duan, S. Fekri, D. Harvey, et al., Water-based quantum dots liquid scintillator for particle physics, 2024, http://dx.doi.org/10.48550/arxiv.2403.10122, arXiv preprint arXiv:2403.10122.

[57] J. Zhou, M. Ge, Y. Han, J. Ni, X. Huang, S. Han, Z. Peng, Y. Li, S. Li, Preparation of biomass-based carbon dots with aggregation luminescence enhancement from hydrogenated rosin for biological imaging and detection of Fe3+, ACS Omega 5 (20) (2020) 11842–11848, http://dx.doi.org/10.1021/acsomega.0c01527.

[58] M. Barisik, S. Atalay, A. Beskok, S. Qian, Size dependent surface charge properties of silica nanoparticles, J. Phys. Chem. C 118 (4) (2014) 1836–1842, http://dx.doi.org/10.1021/jp410536n.

[59] A. Sukhanova, S. Bozrova, E. Gerasimovich, M. Baryshnikova, Z. Sokolova, P. Samokhvalov, C. Guhrenz, N. Gaponik, A. Karaulov, I. Nabiev, Dependence of quantum dot toxicity in vitro on their size, chemical composition, and surface charge, Nanomaterials 12 (16) (2022) 2734, http://dx.doi.org/10.3390/nano12162734.

[60] Ł. Janus, J. Radwan-Pragłowska, M. Piątkowski, D. Bogdał, Facile synthesis of surface-modified carbon quantum dots (CQDs) for biosensing and bioimaging, Materials 13 (15) (2020) 3313, http://dx.doi.org/10.3390/ma13153313.

[61] L.E. González-García, M.N. MacGregor, R.M. Visalakshan, A. Lazarian, A.A. Cavallaro, S. Morsbach, A. Mierczynska-Vasilev, V. Mailänder, K. Landfester, K. Vasilev, Nanoparticles surface chemistry influence on protein corona composition and inflammatory responses, Nanomaterials 12 (4) (2022) 682, http://dx.doi.org/10.3390/nano12040682.

[62] H. Xu, X. Yang, G. Li, C. Zhao, X. Liao, Green synthesis of fluorescent carbon dots for selective detection of tartrazine in food samples, J. Agricult. Food Chem. 63 (30) (2015) 6707–6714, http://dx.doi.org/10.1021/acs.jafc.5b02319.

[63] N.A. Alarfaj, M.F. El-Tohamy, H.F. Oraby, CA 19-9 pancreatic tumor marker fluorescence immunosensing detection via immobilized carbon quantum dots conjugated gold nanocomposite, Int. J. Mol. Sci. 19 (4) (2018) 1162, http://dx.doi.org/10.3390/ijms19041162.

[64] A.F. Shaikh, M.S. Tamboli, R.H. Patil, A. Bhan, J.D. Ambekar, B.B. Kale, Bioinspired carbon quantum dots: an antibiofilm agents, J. Nanosci. Nanotechnol. 19 (4) (2019) 2339–2345, http://dx.doi.org/10.1166/jnn.2019.16537.

[65] A. Dager, T. Uchida, T. Maekawa, M. Tachibana, Synthesis and characterization of mono-disperse carbon quantum dots from fennel seeds: photoluminescence analysis using machine learning, Sci. Rep. 9 (1) (2019) 14004, http://dx.doi.org/10.1038/s41598-019-50397-5.

[66] J. Tang, J. Zhang, Y. Zhang, Y. Xiao, Y. Shi, Y. Chen, L. Ding, W. Xu, Influence of group modification at the edges of carbon quantum dots on fluorescent emission, Nanoscale Res. Lett. 14 (2019) 1–10, http://dx.doi.org/10.1186/s11671-019-3079-7.

[67] L. Li, H. Wang, J. Ye, Y. Chen, R. Wang, D. Jin, Y. Liu, Mechanism study on nanoparticle negative surface charge modification by ascorbyl palmitate and its improvement of tumor targeting ability, Molecules 27 (14) (2022) 4408, http://dx.doi.org/10.3390/molecules27144408.

[68] S.H. Adrita, K.N. Tasnim, J.H. Ryu, S.M. Sharker, Nanotheranostic carbon dots as an emerging platform for cancer therapy, J. Nanotheranostics 1 (1) (2020) 58–77, http://dx.doi.org/10.3390/jnt1010006.

[69] D. Ozyurt, M. Al Kobaisi, R.K. Hocking, B. Fox, Properties, synthesis, and applications of carbon dots: A review, Carbon Trends (2023) 100276, http://dx.doi.org/10.1016/j.cartre.2023.100276.

[70] S. Zhao, G. Yue, X. Liu, S. Qin, B. Wang, P. Zhao, A.J. Ragauskas, M. Wu, X. Song, Lignin-based carbon quantum dots with high fluorescence performance prepared by supercritical catalysis and solvothermal treatment for tumor-targeted labeling, Adv. Compos. Hybrid Mater. 6 (2) (2023) 73, http://dx.doi.org/10.1007/s42114-023-00645-0.

[71] X. Liu, S. Zhao, X. Chen, X. Han, J. Zhang, M. Wu, X. Song, Z. Zhang, The effect of lignin molecular weight on the formation and properties of carbon quantum dots, Green Chem. 26 (6) (2024) 3190–3201, http://dx.doi.org/10.1039/D3GC04694J.

[72] P. Li, L. Sun, S. Xue, D. Qu, L. An, X. Wang, Z. Sun, Recent advances of carbon dots as new antimicrobial agents, SmartMat 3 (2) (2022) 226–248, http://dx.doi.org/10.1002/smm2.1131.

[73] C. Ji, W. Xu, Q. Han, T. Zhao, J. Deng, Z. Peng, Light of carbon: Recent advancements of carbon dots for LEDs, Nano Energy (2023) 108623, http://dx.doi.org/10.1016/j.nanoen.2023.108623.

View publication stats